Joint Centre for Mesoscale Meteorology, Reading, UK

Observations of Oblate Hail Using Dual Polarisation Radar and Implications for Hail Detection Schemes

A. J. Illingworth
T. J. Smyth
T. M. Blackman

Internal Report No. 93

September 1998

Met Office Joint Centre for Mesoscale Meteorology Department of Meteorology
University of Reading PO Box 243 Reading RG6 6BB United Kingdom
Tel: +44 (0)118 931 8425 Fax: +44 (0)118 931 8791
www.metoffice.com

Designed and produced by the Met Office © Crown copyright 2001 01/0240 The Met Office logo is a registered trademark.

Observations of Oblate Hail Using Dual Polarisation Radar And Implications for Hail Detection Schemes

T. J. Smyth, T. M. Blackman and A. J. Illingworth

JCMM, Department of Meteorology, University of Reading, UK

September 24, 1998

* Current affiliation: Tim Smyth, Plymouth Marine Laboratory, Prospect Place, Plymouth PL1 3DH. email: T.J.Smyth@pml.ac.uk

Abstract

Coincidental radar measurements together with *in situ* ground truth observations of large, oblate hail has allowed new insights into the fall mode of oblate hailstones. The effect of the fall mode upon hail detection algorithms using multiparameter radar is investigated and discussed as is the vexed problem of extracting realistic rainfall rates in regions where hail and rain coexist. Observations presented here show that oblate hail can be associated with non-zero values of differential reflectivity, Z_{DR} , which together with the coincidental values of the linear depolarisation ratio, LDR , suggest some degree of alignment. Although large hail can dominate backscatter through the diameter to the sixth power dependence, even if it is aligned it makes a negligible contribution to specific differential phase, K_{DP} . Rainfall rates extracted using K_{DP} in the presence of hail are more robust than those using the contaminated Z_H and Z_{DR} measurements, but proposed hail detection algorithms which compare the observed values of K_{DP} and Z_H do seem error prone. The hailstones measured in this study were of sufficient dimensions to allow Mie scattering to occur at S-band ($\lambda = 9.75$cm). This served to complicate the interpretation of the differential phase measurements. A new hail detection algorithm has been formulated which compares the differential phase predicted from Z_H and Z_{DR} with that actually observed. This avoids the problem of estimating K_{DP} from the derivative of a noisy differential phase profile.

1 Introduction

The differentiation between rain and hail has been a long standing objective of radar meteorologists. Various methods with differing degrees of sophistication have been suggested. The first attempts used reflectivity only measurements. Mason (1971) suggested a 55dBZ reflectivity threshold as an indicator of the presence of hail. Waldvogel *et al.* (1979) describe a method involving the maximum reflectivity, the height of the 45dBZ level above the 0°C isotherm and the vertical reflectivity profile. An automatic hail detection algorithm is currently being advocated for use on the U.S. Next-Generation Weather Doppler Radar (NEXRAD) (Kessinger *et al.*, 1995) which is based upon an examination of the echo intensity and its evolution within the storm. It essentially involves recognising an echo greater than 55dBZ in the mid-level of the cloud. The procedure is complex and no information is provided about the location and extent of the hail fall. This is the greatest problem for all hail detection techniques which rely solely upon reflectivity. The presence of hail can only be inferred in a gross sense, large hail giving a larger value of Z than rain due to the D^6 weighting with differences in the refractive index of ice and liquid water introducing further uncertainty. Another operational algorithm has been formulated by Hardaker and Auer (1994) which combines satellite Infra Red (I.R.) cloud top temperature and radar reflectivity to delineate between hail and rain.

Lemon (1995) postulated the use of a Mie scattering artifact, called a three body scatter spike, for operationally forecasting large hail. This is a weaker echo radially aligned behind a highly reflective (> 63dBZ) echo core. It is found almost exclusively aloft, has low reflectivity (< 20dBZ) and is relatively short (< 8km). Zrnić (1987) examined the radar artifact and explained that this radar echo feature is the result of a triple reflection from the hail shaft. Mie scattering at S-band would occur for particles larger than about 7mm.

Another approach to hail detection has made use of dual-wavelength radar (e.g.Atlas and Ludlam, 1961) where Mie scattering by large hail leads to reduced reflectivity at the shorter wavelength. Dual wavelength studies are plagued with the difficulty of distinguishing between reduced Z due to Mie scattering and attenuation effects at the shorter wavelength and the very different backscatter from wet and dry hail.

Dual-polarisation methods that distinguish rain from hail assume that hailstones, even if oblate, tumble as they fall and appear isotropic to the radar. Bringi *et al.*

(1984) using a dual-polarisation technique found that in regions of hail Z_{DR} rapidly drops to values near 0dB but exhibits larger positive values in the surrounding rain regions. The reflectivity either increases or maintains a relatively high value in the hail. Using distrometer measurements Aydin *et al.* (1986) simulated values of Z_H and Z_{DR} . They found that the raindrop size distributions fell within a well defined region of Z_H - Z_{DR} space. From these distrometer results an empirically derived hail signal (H_{DR}) algorithm was formulated as a measure of the departure of the observed Z_H from the hail-rain boundary. The algorithm took the following form:

$$H_{DR} = Z_H - f(Z_{DR}) \tag{1}$$

$$f(Z_{DR}) = \begin{cases} 27, & Z_{DR} \leq 0(dB) \\ 19Z_{DR} + 27, & 0 \leq Z_{DR} \leq 1.74(dB) \\ 60, & Z_{DR} > 1.74(dB) \end{cases}$$

Positive values of H_{DR} should indicate hail but the derivation of the precise position of the hail demarcation line on a Z_H /Z_{DR} plot is not clear.

The algorithm also implies that the hail medium is isotropic; but the very fact that hailstones are often oblate suggests that they cannot always tumble randomly. In these cases there must be a degree of anisotropy in the falling hailstone population. Recent studies into the detection of hail within rain-hail mixtures have made use of specific differential phase (e.g.Aydin *et al.*, 1995) which are discussed in the next section.

In this paper we report in detail on coincidental multi-parameter radar and *in situ* measurements of a summer hailstorm which occurred in southern England on 10 July 1995.

2 Theory of Polarisation Radar Parameters.

Four radar parameters were used in this study to detect the hail; reflectivity factor, Z_H , differential reflectivity, Z_{DR} , linear depolarisation ratio, LDR , and the differential phase shift, ϕ_{DP} .

a) Measured Polarization Parameters

Differential reflectivity is defined as (Seliga and Bringi, 1976) :

$$Z_{DR}(dB) = 10log_{10}\frac{Z_H}{Z_V} \tag{2}$$

where Z_H and Z_V are the backscattered reflectivity in the horizontal and vertical polarisations respectively. Z_{DR} is a measure of the reflectivity weighted oblateness

(Jameson, 1983) . Raindrops are oblate to a degree which increases with size, and fall with their minor axis oriented vertically so high positive values of Z_{DR} are associated with large oblate raindrops. Regions containing ice particles are usually characterised by lower values of Z_{DR} , despite any asphericity, because of their lower refractive index and tendency to tumble. The Aydin *et al.* (1986) hail detection algorithm relies on hail being isotropic and having lower values of Z_{DR} than would be the case with rain.

The polarisation parameter LDR can be used to distinguish between different hydrometeors. It is defined as:

$$LDR(dB) = 10log_{10}\frac{Z_{VH}}{Z_H} \tag{3}$$

where Z_H is the normal copolar return measured with horizontal polarisation and Z_{VH} is the cross-polar return measured in the horizontal for a vertically polarised transmitted signal. LDR senses oblate particle fall mode; values of LDR above Chilbolton's antenna limit of -32dB occur for particles which cant or tumble as they fall. In essence, only hydrometeors that have axes of symmetry that are canted with respect to the incident polarization will depolarize; because water has a higher dielectric constant than dry ice, the differences in the induced dipoles along the axes of the oblate wet particles are much larger, and so such wet particles have much higher values of LDR.

The differential phase shift, ϕ_{DP} , is the difference in phase between the copolar radar returns measured with vertical and horizontal polarisation $(\phi_V - \phi_H)$. ϕ_{DP} is made up of three contributions; the range-integrated specific differential phase (K_{DP}), differential phase shift on backscatter (δ) and a hardware offset (ϕ_o) which should be constant.

$$\phi_{DP}(r) = \phi_o + \delta(r) + \int_0^r K_{DP}(r')dr' \qquad (^\circ) \tag{4}$$

where r is the range.

K_{DP} is the two-way specific differential phase. As the incident wave propagates through a region of oblate raindrops the horizontally polarised wave lags progressively behind the vertical one so $(\phi_V - \phi_H)$ continually increases and its gradient, K_{DP} , is positive.

Sachidananda and Zrnić (1987) proposed that the two-way K_{DP} (in $^\circ$ km^{-1}) at S-band is related to the rainfall rate (in mmhr^{-1}) by

$$K_{DP} = 0.0308R^{1.15} \tag{5}$$

based on the drop shapes of Green (1975) and an exponential rain drop size spectrum of the form:

$$N(D) = N_0 exp(-3.67/D_0) \qquad (m^{-3}mm^{-1}) \tag{6}$$

with a value of N_0=8000m^{-3}mm^{-1}. Both K_{DP} and R scale linearly with N_0 but because of the low power of the exponent in equation 5 the relationship between K_{DP} and R should be relatively insensitive to changes in N_0.

We shall use the relationship derived by Blackman and Illingworth (1994)

$$K_{DP} = 0.012R^{1.37} \qquad (^{\circ}km^{-1}) \tag{7}$$

for N_0=8000m^{-3}mm^{-1} based on slightly different drop-shapes where the axial ratio r, is related to the diameter D in mm, given by:

$$r = 1.075 - 0.065D - 0.0036D^2 + 0.0004D^3 \tag{8}$$

for drops above 1.1mm size, and an axial ratio of unity for drops smaller than 1.1mm as proposed by Goddard *et al.* (1995) from the radar-distrometer comparisons of Goddard *et al.* (1982) and subsequently supported by the theoretical work of Beard and Chuang (1987). In this case, for these "new" drop shapes, because the exponent in equation 7 is 1.37 the relationship between K_{DP} and R is much more sensitive to changes in N_0 in the drop size spectrum.

At S-band, the differential backscatter component of ϕ_{DP} , δ , is usually considered to be very small as it only occurs in the Mie regime, that is for raindrops or hailstones larger than 7mm, and is only measurable if the hydrometeors have a preferred orientation (McCormick *et al.*, 1979) , but not if randomly oriented. In this paper we confirm the results of Zrnić *et al.* (1993) that the neglect of δ is not a valid assumption, even at S-band, for large, wet, oblate hailstones that have an aligned fall mode. It is important to note that δ , being a backscatter effect, is a transitory change in ϕ_{DP} superposed on the general propagation effect, and can introduce ambiguity in the interpretation of the signal. The ϕ_0 contribution from the hardware is constant and can be subtracted.

b) Simple Models of the Differential Phase Shift on Backscatter

Figure 1 shows the variation of δ with increasing diameter for spongy hail (30% water) at axial ratios of 0.4, 0.6 and 0.8 aligned with a vertical minor axis, calculated using T-matrix code (Waterman, 1965) . The scattering computations were carried out using a refractive index of a water and ice mixture calculated by the Bruggemann rule

(O'Brien and Geodecke, 1988) . For 20mm diameter spongy hail with an axial ratio between 0.4 and 0.6, δ is between -10° and -20° , but δ can be as large as +50° for a 25mm diameter hailstone. Dry ice (ϵ_r = 3.18 + 0.02i at 9.75cm and 0°C Liebe *et al.* (1989)), with a smaller dielectric constant than liquid water (ϵ_r=79.30+25.70i), gives much lower values of δ in the size range 0 to 35mm in diameter. The values of δ for water as a function of diameter and axial ratio are shown in figure 2. (For dry ice δ is a monotonic fuction of size reaching +7° for a 25mm diameter hailstone with an axial ratio of 0.6). Equation 8 indicates that 8mm raindrops have an axial ratio of 0.52, and so would, if monodispersed, produce δ of about -10° .

c) K_{DP} of hail

In an anisotropic medium, such as rain, where the hydrometeors are oblate spheroids with their minor axes oriented in the vertical, ϕ_{DP} increases with range. If hail is assumed to be isotropic then it does not contribute to ϕ_{DP} . Figure 3 shows the variation of K_{DP} with increasing diameter for wet hailstones, axial ratio = 0.6, present in concentrations of $1m^{-3}$, with its major axis *aligned* in the horizontal; negative values arise because of Mie scattering. A single 10mm hailstone per m^{-3} would give a Z of 60dBZ, whereas 21.5mm size would yield 80dBZ. Cheng and English (1983) in an observational study, empirically derived a gamma size distribution for hailstone concentration. They showed that large hailstones are typically present in smaller concentrations than small hailstones. For example they found that a 20mm diameter hailstone has a maximum concentration of $6x10^{-3}m^{-3}$ whereas a 10mm hailstone has a concentration an order of magnitude larger. Large hailstones tend to dominate the reflectivity ($\propto D^6$); taking the example of the monodispersed 20mm hailstone, concentration(N)=$6x10^{-3}m^{-3}$, results in Z_H =56dBZ and a K_{DP} of only 0.06° km^{-1} . In short large hailstones give large values of reflectivity but negligible values of K_{DP} . This implies that lower values of K_{DP} coincidental with high values of reflectivity indicate an increased probability that the precipitation contains hail (Balakrishnan and Zrnić, 1990) . Balakrishnan and Zrnić showed that it was possible to distinguish the mixed phase precipitation from either pure rain or pure hail by using Z_H and K_{DP} and infer the thermodynamic phase and orientation from Z_H and Z_{DR} .

They derived a relationship between K_{DP} (two way) and Z_H in pure rain from equation 5:

$$Z(dBZ) = 44 + 13.86log(K_{DP}) \qquad (9)$$

by assuming an exponential raindrop size spectra (equation 6) with N_0=8000$m^{-3}mm^{-1}$. Two observational studies, consistent with theory, allowed them to conclude that K_{DP} yielded a good estimate of rain liquid water in a rain-hail mixture (they asserted that pure dry hail, as it is nearly isotropic with a small refractive index should not contribute to K_{DP}). They also stated that Z_{DR} of a mixture of rain and hail is completely dominated by the Z_{DR} of the hail (as is the case for Z_H); Z_{DR} they postulated, could provide the necessary information concerning the orientation of the hail. Initially, Balakrishnan and Zrnić proposed an empirical relationship of the form

$$Z(dBZ) = 49 + 8log(K_{DP}) \tag{10}$$

as the boundary to distinguish pure rain from mixed phase and hail, which is clearly in error; for values of K_{DP} above 7° km^{-1} it predicts Z values lower than equation 9 which is their equation for pure rain. They then suggested that an empirical relationship between the hail/rain boundary was given by a value of Z some 7dB higher than in equation 9; this 7dB offset was to some extent confirmed by Ryzhkov and Zrnić (1994):

$$Z(dBZ) = 51 + 13.86log(K_{DP}) \tag{11}$$

Equation 6 based on the Goddard *et al.* (1982) drop shapes leads to a relationship of the form:

$$Z(dBZ) = 45.2 + 11.2log(K_{DP}) \tag{12}$$

for rain with a value of N_0=8000$m^{-3}mm^{-1}$. In figure 4 are plotted equation 9 (dash-dot line) together with the additional 7dB hail threshold curve (equation 11, dotted line) and also equation 12 (solid line). Earlier we pointed out that the exponent 1.37 in equation 7 based on the "new" drop shapes leads to a K_{DP} - R relationship which is more sensitive to the value of N_0 for the drop spectra. In figure 4 the three solid lines are for values of N_0 of 800(upper), 8000(mid) and 80000(lower) $m^{-3}mm^{-1}$; these factor of ten ranges encompass the natural variability of the observed values of N_0 in rain (e.g., Waldvogel, 1974) . This figure confirms the degree of uncertainty in the precise identification of hail from simultaneous Z-K_{DP} observations.

Aydin *et al.* (1995) demonstrated the capability of K_{DP} for estimating rainfall rates in a severe storm with rainfall accompanied by hail (diameter 15-20mm). Using K_{DP} - R relationships they found remarkably good agreement between the radar and *in situ* rain-gauge measurements. The accumulated rainfall was within 10% of the radar estimates, showing that K_{DP} is effective for estimating R in the presence of hail.

Large hailstones make a negligible contribution to the propagation component of ϕ_{DP} but, if wet, the contribution of differential phase shift on backscatter, δ , can have a large but transient effect on ϕ_{DP} (figures 1 and 2). Hailstones may attain such a size as to produce backscatter effects in the Mie regime even at S-band. This then would invalidate the assumption that the value of ϕ_{DP} is attributable entirely to the propagation component K_{DP} . Melting hail can produce differing effects on the various radar parameters. Aydin and Zhao (1990) in a theoretical study, predicted that well oriented partially melted hailstones of moderate size (about 30mm) could produce low positive Z_{DR} combined with large transient increases in the observed ϕ_{DP} due to pronounced Mie effects. In an observational study using both the WSR-88D radar and the nearby dual polarised radar at Cimarron, Zrnić *et al.* (1993) used δ to categorise hail size. δ fluctuates rapidly and changes sign over a narrow size band. They observed a persistent negative δ feature and attributed it to horizontally oriented water coated oblates of size between 8 and 16mm. It must be noted here that δ is very sensitive to changes in the composition of the hailstones.

Zrnić *et al.* (1993) assumed δ was transient and could be removed by filtering which then left a standard error of 3-5° in the derived value of ϕ_{DP} . K_{DP} is the derivative of ϕ_{DP} and so becomes quite noisy especially when attempts are made to estimate it over short distances. These uncertainties can make it difficult to apply equations 10, 11 and 12 in practice.

3 Hailstone Fall Mode

Knight (1986) stated that the tumbling motion determines the average orientation of the long dimension, be it in the vertical, horizontal or a random direction. This in turn would have an effect on the polarisation on backscatter of the radar signal. The fall mode of hailstones is therefore of crucial importance in the polarimetric radar detection of hail, and it is an area where there is little consensus of opinion.

Bringi *et al.* (1984) and Aydin *et al.* (1986) assume that the hail medium is isotropic. This is consistent with the findings of Knight and Knight (1970) who, in their detailed examination of the falling behaviour of hailstones, concluded that oblate hailstones tumble rapidly as they fall and grow with no strong orientation effect. Using circular polarisation radar, Hendry and Antar (1984) showed that the degree of common alignment of hail is generally much smaller than that of rainfall.

Hailstones display a wide variety of shapes which implies that there are a great number of different fall modes. The most common shape is that of an oblate spheroid (Browning and Beimers, 1967) . These oblates even display a degree of triaxiality (Thwaites *et al.*, 1977) . Thwaites *et al.* found that the ratio of the major to minor axes was between 0.3 and 1, the mean value being between 0.6 and 0.8. Large oblate hailstones could produce a considerable departure from the hail signatures of Bringi *et al.* (1984) and Aydin *et al.* (1986) if they were preferentially oriented.

Zrnić *et al.* (1993) assumed that both large oblate and prolate hailstones would tend to be vertically oriented, that is with the minor axis in the horizontal. They speculated that hail with diameters larger than about 2cm would produce Z_{DR} values of around -1dB. Illingworth *et al.* (1987) reported one example of a region of negative Z_{DR} of about 1km in size at a height of 5km with values down to -1dB, which was coincidental with the 60dBZ contour, but it was very transitory and only lasted a few minutes. Negative values of Z_{DR} imply that the hail has a vertical fall mode. This is consistent with the theoretical calculations of Kry and List (1974). One class of solution they termed symmetric gyration. Thwaites *et al.* (1977) considered this to be the most general fall mode of hailstones and used it as a basis for their experimental work. They grew artificial hail to a similar shape and structure to that of natural oblate hail by attaching a spherical embryo to a rotating axle and at the same time causing the minor axis to move in a conical manner about the horizontal. They inferred that if naturally oblate hail grows during this type of motion, triaxiality could be produced using elliptical rather than a symmetrical cone of motion. In the limiting case the minor axis would be in the horizontal and hence produce the negative values of Z_{DR} .

List (1959) carried out experiments in a water tank using oblate spheroids. He concluded that oblate hail falls with the shortest axis vertical acquiring maximum drag and minimum speed. This would lead to positive values of Z_{DR} . Browning and Beimers (1967) argued that if this fall mode continued then the resulting hailstone growth would very quickly become asymmetric, this being contrary to observation. They postulated that symmetry is preserved by the hailstone occasionally flipping over although Knight and Knight (1970) stated that to produce such excellent symmetry as is often observed the hailstones would have to flip very quickly. Oblate hailstones oriented in the manner described here would give a positive value of Z_{DR} and, depending upon the degree of oblateness and size of the hailstones, would if wet produce a differential phase shift on

backscatter (δ). This would only be manifested though if the hail medium throughout the pulse volume had a preferred orientation (e.g.McCormick *et al.*, 1979) .

4 Observations

We report on coincidental multi-parameter radar and *in situ* measurements of the precipitation produced by a summer hailstorm that developed and grew in southern England on 10 July 1995. The hailstorm was remotely sensed by the S-band ($\lambda = 9.75cm$) Chilbolton radar which has Doppler and polarisation capability (Goddard *et al.*, 1994b) and a narrow (0.28°) beam width allowing excellent resolution of the storm structure.

The hailstorm formed in conditions favouring vigorous convection. The maximum temperatures in the area were around 30°C and a nearby upper air ascent revealed considerable instability aloft favouring conditions for deep convection to occur. The adiabatic liquid water content (LWC) was calculated from the ascent and found to be 14gm^{-3} . Both high LWC and strong vertical updrafts are important factors in the production of large hail (e.g.List, 1985) .

The storm was tracked for about 30 minutes (between 1700 and 1730UTC) roughly corresponding to a track 10km long, starting about 15km to the southwest of the town of Reading (Berkshire) and moving through its western districts and then north and east. The storm moved at 20kmhr^{-1} in a broadly northerly direction, although individual cells had a more north-easterly trajectory.

The radar data was coincidental with ground *in situ* verification of the presence of hail by more than 80 observers in the Tilehurst area of Reading and by the collection of 55 hailstones. This aided the interpretation of the various radar parameters and has allowed various hail detection algorithms to be tested. The hailstones were transported to a cold room so that structural descriptions and measurements of size and degree of oblateness could be made. Closer examination of the radar data has allowed an insight into the fall mode of the hailstones which is a determining factor in their resulting shape.

a) Ground Truth Hail Observations

Figure 5 shows the ground observations of hail which extended in a swath about 20km long and around 3km wide, although the exact extent would be harder to verify as the areas to the west and south of Calcot are more sparsely populated. Hail-only observations (a period during the storm's passage over the observation point where the

precipitation was purely hail) were situated on the eastern edge of the storm. In this region observers reported the hail to be larger than that observed further west, and shaped like a lozenge or disc. Satellite and radar observations showed that the storm moved in a north-northeasterly direction so the map gives a time integrated picture; the hail being observed in Burghfield some 20 minutes before the Tilehurst environs. Disc shaped hail was also reported at Burghfield and these were saved for analysis. The general storm sequence over Tilehurst (apart from the eastern fringe) was a period of torrential rain followed by large disc shaped hail falling and then another period of rain. The whole sequence lasted between 10 and 15 minutes. Damage was reported at several locations. Holes were made in corrugated plastic roofing where the hail had attained sufficient size and terminal velocity. Cars were also dented and leaves were stripped from plants and trees. Photographic evidence of hail lying on the ground shows that there was a remarkably low number concentration ($N \sim 100 m^{-2}$) which ground based observers confirmed fell in a period of 5 minutes with no accompanying rain.

55 hailstones were collected from Burghfield (see figure 5). Upon measurement in a cold room they were found to be similar in dimensions and shape to those observed at Tilehurst. Figure 6 shows a photograph of one of the hailstones collected. It has been cut in half so that the interior can be examined more closely. The hailstone is oblate rather than prolate and contains a well defined approximately circular embryo surrounded by several growth rings of alternate wet (transparent ice) and dry (milky ice) growth regimes (Johnson and Rasmussen, 1992) . The hailstone shown represents the typical size observed during this storm, being 2.2cm in the major axis with an axial ratio (major to minor) of 0.6. The largest hailstones measured had a major axis of 3.2cm. The structure of the hailstones was remarkably similar suggesting that the hailstones originated and passed through the same regions of the storm. Wet growth was also apparent in regions of cloudy ice in some hailstones. We speculate that this occurs when unfrozen water is built into and stabilised by the growing ice framework, the rate of heat transfer being insufficient to freeze the large quantities of supercooled water collected.

b) Radar Observations

For the radar observations we focus on a single PPI (1720 UTC) which best captures the relevant differential scattering signatures in the lower levels of the storm in plan view. We will also focus on two particular rays (37.8° and 29.38°) in the storm to

quantitatively interpret the scattering signatures.

(i) Guide to significant features of PPI

Figure 7 shows a horizontal radar scan (PPI) within a minute or so of the time of the hail observations in the Tilehurst (27E 35N of radar) area. The height of the radar cross section at a range of 45km is 700m, 2.3km below the melting layer.

The area where $Z_{DR} > 3$dB tends to follow the 50dBZ contour as would be expected for heavy rain, but where Z > 60dBZ at 26E 34N, Z_{DR} dips below 2dB; if this were pure rainfall the low value of Z_{DR} implies an unrealistic rainfall rate of $\sim$1000mmhr^{-1} so we infer the presence of mixed rain and tumbling hail. The Z_{DR} does not drop to zero, which would be indicative of purely tumbling hail, but instead either the hail component has some degree of alignment or the rain component acts to raise the value of Z_{DR} .

The region where the large oblate hail was observed to fall is near 28E 35N. Here Z_{DR} is about 3$\rightarrow$ 5dB. This suggests that the oblate hailstones were not randomly tumbling as they fell, but rather had a systematic fall mode with their major axis in the horizontal. Here Z_H is between 40 and 60dBZ which is consistent with the low number density of hailstones observed at the ground, given their exceptional size.

As we use an internally consistent (reflectivity) calibration technique that assumes a pure rain medium, we must identify a part of the scan where we are confident of rain-only echoes. The precipitation in the NW quadrant of figure 7 is all rain as confirmed by the values of LDR below -28dB, and the monotonically rising ϕ_{DP} giving two-way K_{DP} values in the heaviest precipitation of about 16° km^{-1} indicating rainfall rates of nearly 200mmhr^{-1} . Range profiles through this region were used for the absolute calibration of the radar (see figure 10). This is discussed in section 5.

(ii) Ray Profile through Hail-Bearing Regions

The observations in the eastern half of figure 7 are more complicated as the ray profile in figure 8 demonstrates. The ϕ_{DP} profile was generated by taking the mean of four separate rays through the region containing hail. As each ray has a beamwidth of 0.28° this results in a sample width of nearly 1km at the range of the hailstorm. Using this method the noise in ϕ_{DP} is reduced and the equivalent of a 1 second dwell is obtained (calculated from the slew rate of the dish).

The small region at 26E and 32N ('A' in figure 8) where ϕ_{DP} falls 7$\rightarrow$ 10° (see figure 2) below the system value of -27° and Z_{DR} exceeds 5dB, cannot be a propagation

effect, but must be due to differential phase shift on backscatter. This is consistent with monodispersed 7→ 8mm diameter raindrops which have very little canting, a conclusion confirmed by the low value of LDR . Region B in figure 8 exhibits the classic signature of a Z_{DR} 'dip' due to tumbling hail (or conceivably with a degree of alignment) mixed with rain.

Region C is the region centred on 28E and 36N in figure 7 where ϕ_{DP} becomes noisy and is coincident with the ground observations of oblate hail. LDR has risen somewhat and Z_{DR} is between 2 and 4dB; this strongly suggests oblate hailstones large enough to undergo Mie scattering, with a spread of canting angles to give the observed LDR . The lower Z_H value in a region of large hailstones is consistent with their low concentration (Mie scattering would reduce Z_H further). Such a low concentration cannot produce significant K_{DP} , so we interpret the total differential phase shift values as local deviations superimposed on a trend (increasing phase difference), indicating large negative values of δ (-10°) due to wet oblate hail, with a degree of alignment (figure 1). Because of the very narrow radar beamwidth it is unlikely that reflectivity gradients are degrading the phase measurements.

In region B (and by extrapolation the first half of C) the value of K_{DP} is 14° km^{-1} (indicating a rainfall rate of about 180mmhr^{-1} from equation 5 or equation 7) accompanied by values of Z_H which are close to 60dBZ. Figure 4 and equation 9 would predict the rain component having a value of Z_H close to 60dBZ, but equation 12 suggests a slightly lower value of Z_H , but if the rain has N_0 of 800 or 80000$m^{-3}mm^{-1}$ the values could be 62 and 57dBZ respectively. This uncertainty in the values of Z_H for a given rainfall rate highlight the difficulties of using equation 11 as a hail criterion. In this case to trigger the algorithm, Z_H would need to be >67dBZ, yet the low values of Z_{DR} observed clearly indicate the presence of hail. For pure rain, a rainfall rate of 180mmhr^{-1} and a Z_H of 60dBZ should be accompanied by Z_{DR} values of 3.5dB.

In region D, LDR rises to -18dB which is indicative of wet oblate hail, and Z_{DR} has values of 2-3dB which is consistent with an aligned fall mode with the major axis on average in the horizontal with a 20° canting angle (for an axial ratio of 0.6). Because LDR at the back of the storm reverts to -30dB we feel that these LDR observations are unaffected by propagation and depolarisation of the incident beam. The value of K_{DP} is negligible which suggests that rain was not mixed with the hail and indeed the ground based observations in this region (figure 5) consistently reported a period of just hail

falling and the hailstones being exceptionally large and oblate. The hail is wet because the air temperature is above 0°C .

We are suggesting that region D contains hail, but it is rather difficult to apply the hail criterion of Balakrishnan and Zrnić (1990) in this region because δ leads to an uncertainty in the value of K_{DP} . If K_{DP} is 0.1° km^{-1} or 1° km^{-1} then equation 11 predicts hail if Z_H >37 and 51dBZ respectively. The observed Z_H is lower than either of these two values

c) Satellite Observations

The closest Meteosat I.R. image available in time to the observations is at 1700UTC (figure 9), the hailstorm's position being marked with a cross. The minimum cloud top temperature, which is indicative of the greatest altitude of the storm at this time, is -56°C (the coldest temperatures are -60°C). For the Hardaker and Auer hail algorithm to be triggered, a coincidental reflectivity of 55dBZ is required. The U.K. networked radar situated at Chenies (51.68° N 0.53° W), which has a 2km grid resolution, showed a maximum reflectivity of 56dBZ at this time although determining whether or not the 55dBZ radar and -56°C satellite pixels are exactly coincidental is problematic. This is because the cloud casts a "shadow" in the I.R. satellite image. The distance between the actual and apparent positions of the cloud being a function of the cloud top height and viewing angle of incidence (latitude and longitude dependent) by the satellite's radiometer. In addition wind shear may displace the cold cloud top from above the main precipitation core. The most important function of a hail detection algorithm is to exactly pinpoint the hail. With this method it is only possible to say that there is an increased probability of hail falling somewhere within the storm cell, this being diagnosed by the low cloud top temperatures and high reflectivity.

5 Derived Rainfall Rates

Figure 10 shows a ray profile through the rain in the NW quadrant of the storm shown in figure 7. The parameters shown are the measured and predicted total ϕ_{DP} along the path predicted using the calibration method of Goddard *et al.* (1994a). The effect of adding/subtracting 1dBZ of power from Z_H on the expected K_{DP} is shown. Figure 11 (from Goddard *et al.*, 1994a) is the theoretical basis for the calibration method and shows that the ratio K_{DP} /Z_H as a function of Z_{DR} only varies very slightly as the integer index (μ/m) of the gamma function changes. K_{DP} (specific differential

phase) can be predicted from the (non-attenuated) Z_H and Z_{DR} measurements at each radar range gate. Uncertainties about the form of the gamma distribution are relatively unimportant compared with a change in absolute power calibration of ± 1dBZ. This method can therefore be used to accurately calibrate Z_H to at least within 0.5dBZ especially if long dwell periods are used. (Z_{DR} can be calibrated by using an RHI through the ice phase section of the storm above the melting layer; the values of Z_{DR} at altitudes above the freezing layer within the ice should be very close to 0dB, any offset from this value can be added or subtracted.) Figure 10 shows close agreement between the measured and expected total ϕ_{DP} along the path which confirms that the precipitation is rain. It also implies that we can have confidence in the absolute calibration of Z_H .

Algorithms to detect hail within mixed phase precipitation make use of K_{DP} to extract the relative contributions from rain and hail. (Figure 12 is a ray profile through a different region of the same storm shown in figure 7 some 13 minutes earlier.) Figure 8 and figure 12 show the importance of δ which causes ambiguities in the interpretation of ϕ_{DP} purely in terms of K_{DP} . In region (1) the precipitation volume is filled with a low number density of large raindrops; region (2) a mixture of rain and tumbling hail. The flat gradient in ϕ_{DP} beyond 40km in region (4) is indicative of light rain (the positive Z_{DR} indicating a low concentration of large drops) which gives a very slight contribution to K_{DP} and no δ . This provides a fixed point to quantify the total amount of differential propagation phase shift that has occured through the storm. The dashed line on figure 12, drawn by eye, represents an estimate of the ϕ_{DP} (propagation) response starting at the system offset of -27° which was determined from background ϕ_{DP} values in light precipitation. This provides another fixed point allowing us to deduce that between 37 and 41km the propagation phase shift change due to propagation through the precipitation volume is +23° . The difference between the ϕ_{DP} and K_{DP} profiles is caused by a large negative contribution from δ , suppressing the ϕ_{DP} signal and indicating large oblate wet aligned hail in region (3). The difference between the observed ϕ_{DP} profile (solid line) and the extrapolated (dashed line) is caused by the large negative contribution from δ indicating large oblate wet hail in region(3). Literal interpretation of the jump in the ϕ_{DP} profile as K_{DP} would predict rainfall rates of 325mmhr^{-1} ; clearly incompatible with the observed Z_H of 50dBZ at this point. If we take the extrapolated value of K_{DP} between 38 and 40km range as 8.5° km^{-1} ,

indicating a rainfall rate of about 120mmhr^{-1} , then figure 4 predicts that Z_H should be between 54 and 58dBZ depending upon the N_0 of the rain. The observed value is between 58 and 60dBZ indicating that about half of the echo is probably due to hail. Uncertainties in the value of K_{DP} in the presence of δ limit the precision of this conclusion, but confirmation is provided by values of Z_{DR} below 2dB which are too low for pure rainfall of this intensity.

The largest values of δ in figure 12 are approximately -20° in region (3) which is consistent with spongy hailstones with a diameter of 20mm and an axial ratio of 0.5. We therefore postulate that in region (3) hailstones of this composition and dimensions are present and masking the propagation component of the total differential phase shift and causing ambiguity in its interpretation using K_{DP} . Finite δ can only be produced by hydrometeors with a degree of alignment; additionally the positive values of Z_{DR} (~3dB) imply that the alignment was on average with the minor axis in the vertical. This is consistent with the theories of Browning and Beimers (1967) and suggests that the fall mode is anisotropic, rendering the hail "invisible" to the hail detection algorithm of Aydin *et al.* (1986).

Our analysis of figures 8 and 12 draws attention to the difficulties of deriving rainfall and identifying the presence of hail from Z_H and ϕ_{DP} . Two problems arise. Firstly the ϕ_{DP} profile can be affected by δ , the differential phase shift on backscatter, and secondly the relationship between K_{DP} and rainfall rate (and hence K_{DP} and Z_H for rain) is not unique but depends on an assumed value of N_0 in the raindrop size spectra. In the next section we shall consider how that variables Z_H , Z_{DR} and K_{DP} can be combined. Because K_{DP} and Z_{DR} in rainfall are not independent their very dependence and consistency can be used to calibrate Z_H when rain is known to be present. If the consistency fails then regions where significant hail is present can be identified.

6 New hail detection algorithm

The calibration method of Goddard *et al.* (1994a) could have an application as a viable method for detecting hail as well as providing an accurate method for calibration. Essentially this calibration technique *assumes* only raindrops are present in the scattering volume and then relies on the fact that the value of K_{DP} /Z_H is a unique function of Z_{DR} (figure 11). The calibration of Z_H is adjusted so that the path integrated phase shift, calculated from the theoretical value of K_{DP} at each gate derived from the ob-

served values of Z_H and Z_{DR} , agrees with the observed path integrated phase shift (figure 10). The advantage of this approach is that the path integrated phase shift is used as a constraint and this quantity can be estimated quite accurately. This contrasts with the errors involved in trying to derive K_{DP} from differentiating a very noisy ϕ_{DP} profile. Once the radar is calibrated, then for all paths through rain, the integrated phase shift computed from the observed values of Z_H and Z_{DR} should agree with the observed total change in ϕ_{DP} along the path. Any difference between the measured ϕ_{DP} and the predicted value will indicate a violation of the "rain-only" assumption and should therefore detect the presence of any non-rain precipitation.

Figure 12 shows the total phase shift (dash-dot line) predicted from the observed values of Z_H and Z_{DR} assuming that only rain is present. The total phase shift is massively overestimated; most of the divergence from observations occurring in region 2 where the values of Z_H are high but Z_{DR} is low. If the region was characterised by purely rainfall with a Z_{DR} of 1.2dB and Z_H = 62dBZ, it would imply that there was a large concentration of small raindrops with N_0 200 times the Marshall Palmer value and an implausible rain rate of >1000mmhr^{-1} . However, the integrated phase shift based on the rain assumption, is 50° higher than that observed, confirming that region 2 contains randomly tumbling hail which is depressing Z_{DR} and raising Z_H .

The difference in the observed additional phase shift for each 300m gate and that calculated from Z_H and Z_{DR} at that gate assuming rain to be present is displayed in figure 13 for the data along the ray in figure 12. The observed ϕ_{DP} is quite noisy, so averages over five adjacent rays, each separtated by one degree in azimuth, were taken. This is equivalent to a distance of nearly 1km at this range. The rms noise in observed ϕ_{DP} is typically ±2° and figure 13 indicates that if the difference in the observed and computed change in differential phase shift from one gate to the next is more than 2° then hail is present. In region 2 the theoretical value of the phase shift is greater than that observed by 12° because hail is depressing the value of Z_{DR} . In region 3 the theoretical value is less than that observed by about 8° ; the deviation is negative because the differential phase shift on backscatter from the large hail is depressing the observed phase shift. This hail algorithm can therefore detect hail where other algorithms fail namely where there is a mixture of rain and hail and also where large oblate hail causes finite δ . As a control, the algorithm was tested in regions of moderately heavy rain (Z_H > 40dBZ and where ϕ_{DP} increased monotonically). The

results for a typical rain ray are shown in figure 14 *a) - c)*. The difference between the measured and predicted ϕ_{DP} is less than $\pm 2°$ which confirms that there is no hail along the length of the ray.

Finally, in figure 15 the hail detection algorithm is applied to the PPI data in figure 7. In this figure we have plotted the difference in the theoretical path integrated differential phase shift assuming rain and the observed differential phase shift. In the north-west quadrant the difference is nearly always less than 5° indicating rainfall, whereas in the centre of the plot the difference rapidly increases with range reaching values in excess of 30° behind the hail region. The area deemed to be large raindrops which are accompanied by a negative value of δ shows up as a negative difference between theoretical and observed phase difference of more than 15° . In figure 15 four adjacent rays have been averaged together giving a radial resolution of 1km. In figures 13 and 14 the differences between theoretical and observed phase shift for every 300m gate were computed. For reliable detection figure 15 indicates that it is probably more realistic to use changes of more than 5° between theory and observation occurring over distances of 1km in range as an indication of the presence of hail.

7 Conclusions

This paper has addressed the question of hailstone fall mode as this is of crucial importance in the detection of hail by radar. It is likely that many fall modes exist for hailstones, this being both dependent upon, and a determining factor in, their resulting shape and size. This is forced in turn by the ambient meteorological conditions such as LWC and updraught speed. The established hail detection algorithm of Aydin *et al.* (1986) is reliant upon the hailstones tumbling randomly, resulting in a near zero values of Z_{DR} , for them to be distinguishable from rain. The oblate hailstones observed in the 10 July 1995 storm fell with their major axis on average in the horizontal resulting in Z_{DR} ~3dB and causing the hail detection algorithm to fail. An additional complication is the presence of rain which also contaminates the Z_{DR} signal. This implies that the hailstones had a preferred orientation as they fell. This raises the additional question of how did the hail fall if it did not tumble randomly?

The radar observations are consistent with the oblate hail falling with its largest axis in the horizontal, implied by high values of Z_{DR} , and canting at $\pm$ 10→20° about the horizontal, deduced from LDR . A possible fall mode to be consistent with the radar

observations would be one where the major axis is describing a cone about the horizontal. This is shown in figure 16, and is consistent with the fall mode postulated by Browning and Beimers (1967). To produce the observed hailstone structural symmetry then the hailstone would have to occasionally flip over to allow the supercooled water to accrete on the opposite face of the stone. An alternative fall mode could involve the hailstones rotating about their major axis which would result in symmetry. The resulting hailstones would be prolate though rather than oblate shapes that were observed i.e., more like a cigar than a disc, so this mode can be rejected.

The laboratory experiments of Thwaites *et al.* (1977) grew hail similar in shape and size to that observed on the 10 July 1995, but the fall mode they used to grow the hail is inconsistent with the observed radar response. Their fall mode involved the major axis being, on average, in the vertical which would result in negative Z_{DR} .

The hail identification algorithm of Balakrishnan and Zrnić (1990) relies on converting the observed K_{DP} into a reflectivity component of the rain; if the observed reflectivity is much higher than this then the difference is due to the presence of hail. In practice difficulties arise. Using the "new" drop shapes of Goddard *et al.* (1995) it seems that the conversion form K_{DP} to Z_H is dependent on the value of N_0 in the raindrop size spectrum. If we assume that the value of N_0 can vary up and down by a factor of ten, from as low as 8000 up to 80000$m^{-3}mm^{-1}$, then this introduces an error of a factor of two (3dB) in the Z_H value. This uncertainty means that up to 50% of the echo could be due to hail but would remain undetected. Balakrishnan and Zrnić suggested that values of Z_H 7dB above the value predicted for rain from K_{DP} could be used to identify hail, but this leads to such extremely high values of Z_H that our results indicate it would be rarely triggered even when the presence of hail is confirmed by ground observations. In addition the derivation of K_{DP} from a noisy ϕ_{DP} profile observed along a ray is error prone and is affected by a superposed ϕ_{DP} signal due to differential phase shift on backscatter when the hail is large enough to undergo Mie scattering. Filtering can be used to remove the more obvious spikes due to differential phase shift but this is complicated for extensive regions of large hail.

We suggest that a more reliable approach is to use the consistency of the three observables Z_H , Z_{DR} and K_{DP} in rain. This has been proposed as a calibration technique for rain by Goddard *et al.* (1994b) and relies on the fact that, for rain, K_{DP} /Z_H is a unique function of Z_{DR} . In rain the total differential phase shift found from

the theoretical values of K_{DP} at each gate derived from the observed values of Z_H and Z_{DR} should agree with the observed value of the total differential phase shift along the path. If the theoretical and the observed phase shifts diverge then hail is present. An examination of the Chilbolton data suggests that if five rays are averaged together and ranges of 1km are considered, then a difference in the observed and the calculated differential phase shift of greater than 5° should be a reliable indicator of the presence of hail. The method has the advantage that it does not rely on deriving a value of K_{DP} by differentiating a noisy profile of differential phase with range. Instead it compares the observed total phase shift with one computed from observed values of Z_H and Z_{DR} .

We have suggested that hail algorithms which rely on Z_H /Z_{DR} alone can fail because hail may not tumble randomly and can be associated with finite values of Z_{DR} . The new algorithm proposed in this paper could fail if the shape and degree of alignment of the falling hail is precisely matched so that a combination of rain and hail gives the same triplet values of Z_H , Z_{DR} and K_{DP} as would be observed for rain. We have been unable to find such a combination but it is conceivable that one could occur on very rare occasions. A more serious problem arises due to the contamination of ϕ_{DP} with ground clutter. If 12% of the signal power is due to ground clutter then the error in Z_H and Z_{DR} will be less than 0.5dB and virtually negligible. However, because the ground clutter has random phase if we consider the amplitude of the return signal, a 6% component with random phase will introduce a noise of over 3° to ϕ_{DP} . Accordingly, profiles with random gate to gate noise above this level will indicate clutter contamination and should not be used for the hail detection algorithm.

In conclusion we also note that many operational radars in Europe operate at C-band. The algorithm outlined in this paper should operate reliably at S-band. At C-band attenuation and propagation problems need to be considered. The values of Z_H will be reduced at the far side of the storm if heavy rainfall is encountered along the ray. In addition, differential attenuation by raindrops leads to reduced values of Z_{DR} at the back of the storm so that they become negative. These propagation effects at C-band are a problem to all proposed hail identification algorithms which rely on polarisation parameters: further work is needed if the new algorithm presented in this paper is to be used at C-band.

8 Acknowledgements

This work was supported by NERC "HYREX" grant GST/02/718.

We thank the RCRU group at RAL for allowing access to the Chilbolton radar.

Jothiram Vivekenanden (NCAR) provided the scattering code.

Thanks to Mr. I. Maclean from the University of Reading Library Photographic Services for the hailstone pictures and to Steve Woolnough for spending a whole day at -27°C measuring the hailstones!

Thanks to Chun-Lei Liu for the production of figure 15.

References

Atlas, D. and Ludlam, F. H. (1961). Multiwavelength radar reflectivity of hailstorms. *Quart. J. Roy. Meteor. Soc.*, **87**, 523–534.

Aydin, K. and Zhao, Y. (1990). A computational study of polarimetric radar observables in hail. *IEEE Trans. Geosci. Rem. Sens.*, **28**, 412–422.

Aydin, K., Seliga, T., and Balaji, V. (1986). Remote sensing of hail with a dual linear polarisation radar. *J. Climate Appl. Meteor.*, **25**, 1475–1484.

Aydin, K., Bringi, V. N., and Liu, L. (1995). Rain rate estimation in the presence of hail using S-band specific differential phase and other radar parameters. *J. Appl. Meteor.*, **34**(2), 404–410.

Balakrishnan, N. and Zrnić, D. S. (1990). Estimation of rain and hail in mixed-phase precipitation. *J. Atmos. Sci.*, **47**, 565–583.

Beard, K. V. and Chuang, C. (1987). A new model for the equilibrium shape of raindrops. *J. Atmos. Sci.*, **44**, 1509–1524.

Blackman, T. M. and Illingworth, A. J. (1994). Improved measurements of rainfall using differential phase techniques. In *Cost 75 Weather Radar Systems EUR 16013 EN*, pages 662–671, Brussels, Belgium.

Bringi, V. N., Seliga, T. A., and Aydin, K. (1984). Hail detection with a differential reflectivity radar. *Science*, **225**, 1145–1147.

Browning, K. A. and Beimers, J. G. D. (1967). The oblateness of large hailstones. *J. Appl. Meteor.*, **6**, 1075–1081.

Cheng, L. and English, M. (1983). A relationship between hailstone concentration and size. *J. Atmos. Sci.*, **40**, 204–213.

Goddard, J. W. F., Cherry, S. M., and Bringi, V. N. (1982). Comparison of dual-polarisation radar measurements of rain with ground-based distrometer measurements. *J. Appl. Meteor.*, **21**, 252–256.

Goddard, J. W. F., Eastment, J. D., and Thurai, M. (1994a). The Chilbolton advanced meteorological radar: a tool for multidisciplinary research. *Electronics & Communications Engineering J.*, **6**, 77–86.

Goddard, J. W. F., Tan, J., and Thurai, M. (1994b). Technique for calibration of meteorological radars using differential phase. *Electronics Letters*, **30**, 166–167.

Goddard, J. W. F., Morgan, K. L., Illingworth, A. J., and Sauvageot, H. (1995). Dual-wavelength polarisation measurements in precipitation using the CAMRA and Rabelais radars. In *27th Conference on Radar Meteorology*, Vail, Colorado. Amer. Met. Soc.

Green, A. W. (1975). An approximation for the shape of large raindrops. *J. Appl. Meteor.*, **14**, 1578–1583.

Hardaker, P. J. and Auer, A. H. (1994). The separation of rain and hail using single polarisation radar echoes and IR cloud-top temperatures. *Meteorological Applications*, **1**, 201–204.

Hendry, A. and Antar, Y. N. M. (1984). Precipitation particle identification with centimeter wavelength dual-polarisation radars. *Radio Sci.*, **19**, 115–122.

Illingworth, A. J., Goddard, J. W. F., and Cherry, S. M. (1987). Polarisation radar studies of precipitation development in convective storms. *Quart. J. Roy. Meteor. Soc.*, **113**, 469–489.

Jameson, A. R. (1983). Microphysical interpretation of multi-parameter radar measurements in rain: Part I interpretation of polarisation measurements and estimation of raindrop shapes. *J. Atmos. Sci.*, **40**, 1792–1802.

Johnson, D. B. and Rasmussen, R. M. (1992). Hail growth hysteresis. *J. Climate Appl. Meteor.*, **49**, 2525–2532.

Kessinger, C. J., Brandes, E. A., and Smith, J. W. (1995). A comparison of the NEXRAD and NSSL hail detection algorithms. In *27th Conference on Radar Meteorology*, pages 603–605, Vail, Colorado. Amer. Met. Soc.

Knight, C. A. and Knight, N. C. (1970). The falling behaviour of hailstones. *J. Atmos. Sci.*, **27**, 672–681.

Knight, N. C. (1986). Hailstone shape factor and its relation to radar interpretation of hail. *J. Climate Appl. Meteor.*, **25**, 1956–1958.

Kry, P. R. and List, R. (1974). Aerodynamic torques on rotating oblate spheroids. *Phys. Fluids*, **17**, 1807–1092.

Lemon, L. R. (1995). Recognition of the radar "Three Body Scatter Spike" as a large hail detector. In *27th Conference on Radar Meteorology*, pages 533–535, Vail, Colorado. Amer. Met. Soc.

Liebe, H. J., Manabe, T., and Hufford, G. A. (1989). Millimeter-wave attenuation and delay rate due to clouds/fog conditions. *IEEE AP*, **37**, 1617–1623.

List, R. (1959). Zur aerodynamic von hagelkörnern. *Z. angew. Math. Phys.*, **10**, 143–159.

List, R. (1985). *Thunderstorm Morphology and Dynamics: Ed. Kessler, E.*, chapter 12, pages 259–276. Univ. Oklahoma Press., 2nd edition.

Mason, B. J. (1971). *The Physics of Clouds.* Clarendon.

McCormick, G. C., Allan, L. E., and Hendry, A. (1979). The backscatter matrix of ice samples: its relation to the identification of hail by radar. *J. Appl. Meteor.*, **19**, 77–84.

O'Brien, S. G. and Geodecke, G. H. (1988). Scattering of millimetre waves by snow crystals and equivalent homogeneous symmetric particles. *Applied Optics*, **27**, 2439–2444.

Ryzhkov, A. V. and Zrnić, D. (1994). Precipitation observed in Oklahoma Mesoscale Convective Systems with a polarimetric radar. *J. Appl. Meteor.*, **33**, 455–464.

Sachidananda, M. and Zrnić, D. (1987). Rain rate estimates from differential polarisation measurements. *J. Atmos. Oceanic Technol.*, **4**, 588–598.

Seliga, T. A. and Bringi, V. N. (1976). Potential use of radar differential reflectivity measurements at orthogonal polarisations for measuring precipitation. *J. Appl. Meteor.*, **15**, 69–76.

Thwaites, S., Carras, J. N., and Macklin, W. C. (1977). The aerodynamics of oblate hailstones. *Quart. J. Roy. Meteor. Soc.*, **103**, 803–808.

Waldvogel, A. (1974). The No jump of raindrop spectra. *J. Atmos. Sci.*, **31**, 1067–1078.

Waldvogel, A., Federer, B., and Grimm, P. (1979). Criteria for the detection of hail cells. *J. Appl. Meteor.*, **18**, 1521–1525.

Waterman, P. C. (1965). Matrix formulation of electromagnetic scattering. *Proc. IEEE*, **53**, 805–812.

Zrnić, D. S. (1987). Three-body scattering produces precipitation signature of special diagnostic value. *Radio Sci.*, **22**, 76–86.

Zrnić, D. S., Bringi, V. N., Balakrishnan, N., Aydin, K., Chandrasekar, V., and Hubbert, J. (1993). Polarimetric measurements in a severe hailstorm. *Mon. Weath. Rev.*, **121**(8), 2223–2238.

Captions

Figure 1: Variation of δ for spongy hail (T = 0°C).

Figure 2: Variation of δ for water (T = 0°C).

Figure 3: Variation of K_{DP} for a wet hailstone, axial ratio = 0.6, concentration $1m^{-3}$.

Figure 4: Predicted values of two-way K_{DP} and Z_H for rain and hail. Dash-dot pure rain (Balakrishnan and Zrnić, 1990) ; dotted, pure hail (Balakrishnan and Zrnić, 1990) ; solid, rain for various values of N_0 using "new" drop shapes and equation 12.

Figure 5: Map of the hail observations. The distances North and East (in km) are relative to the Chilbolton radar (51.145° N, 1.437° W).

Figure 6: Cross sectional photograph of a hailstone collected at Burghfield Common.

Figure 7: PPI of storm showing a) Z_H , b) Z_{DR} , c) ϕ_{DP} and d) LDR , at 1720UTC elevation 0.7° . The bold line shows the ray profile of figure 8 and Tilehurst is positioned at 27E 35N of the radar.

Figure 8: Ray profiles of the radar parameters along the bold line in figure 7.

Figure 9: Meteosat I.R. image for 1700UTC.

Figure 10: The Goddard *et al.* calibration technique applied to a ray through the rainfall in the NW quadrant of figure 7 showing the sensitivity of the computed ϕ_{DP} to small changes in the calibration of Z_H .

Figure 11: Theoretical variation of K_{DP} /Z_H with Z_{DR} for different gamma DSDs.

Figure 12: Fields along a ray Az 29.38° .

Figure 13: Difference between the gradients in modelled and measured ϕ_{DP} for same ray as shown in figure 12.

Figure 14: Ray through a region of rain, 10/7/95 1707:37UTC, azimuth 13.4° . a) Z_H and Z_{DR} b) measured and modelled ϕ_{DP} c) Difference between the gradients of modelled and measured ϕ_{DP} .

Figure 15: Performance of the new hail detection algorithm for the PPI data in figure 7. The variable plotted is the difference in the value of ϕ_{DP} along radar rays computed from Z_H and Z_{DR} assuming rain is present and the observed value of ϕ_{DP} along the ray. Where hail is present this diffence changes by more than 5° km^{-1} , but in the rain in the NW quadrant the difference stays below 5° .

Figure 16: Tumbling motion of oblate hailstone viewed side on.

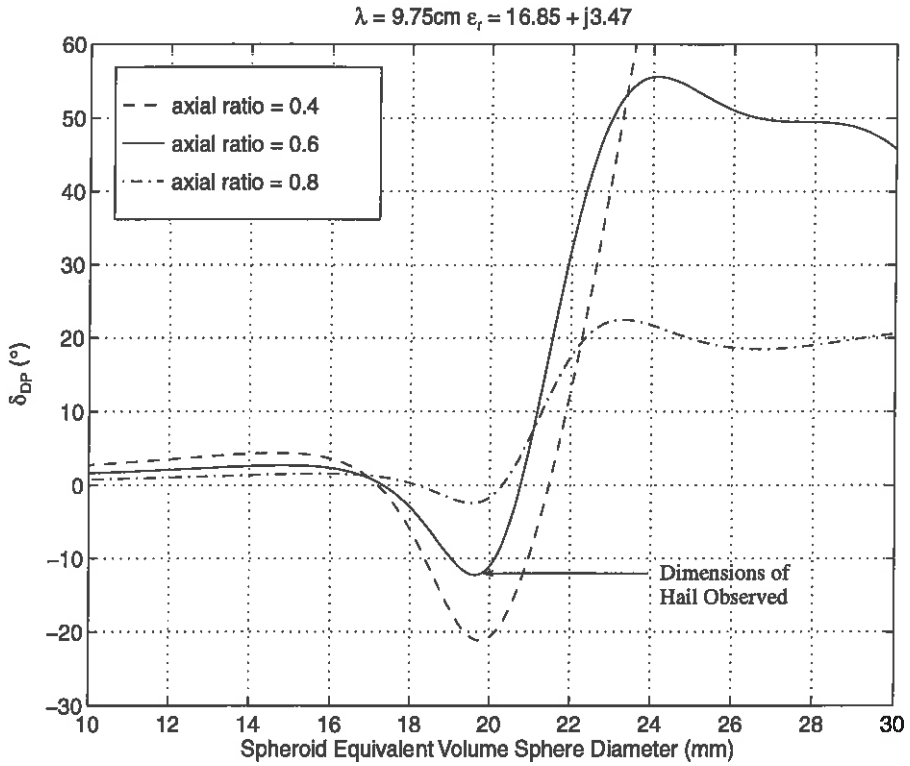
λ = 9.75cm ε_r = 16.85 + j3.47
axial ratio = 0.4
axial ratio = 0.6
axial ratio = 0.8
Dimensions of
Hail Observed
δ_DP (°)
Spheroid Equivalent Volume Sphere Diameter (mm)
60
50
40
30
20
10
0
−10
−20
−30
10
12
14
16
18
20
22
24
26
28
30

Figure 1:

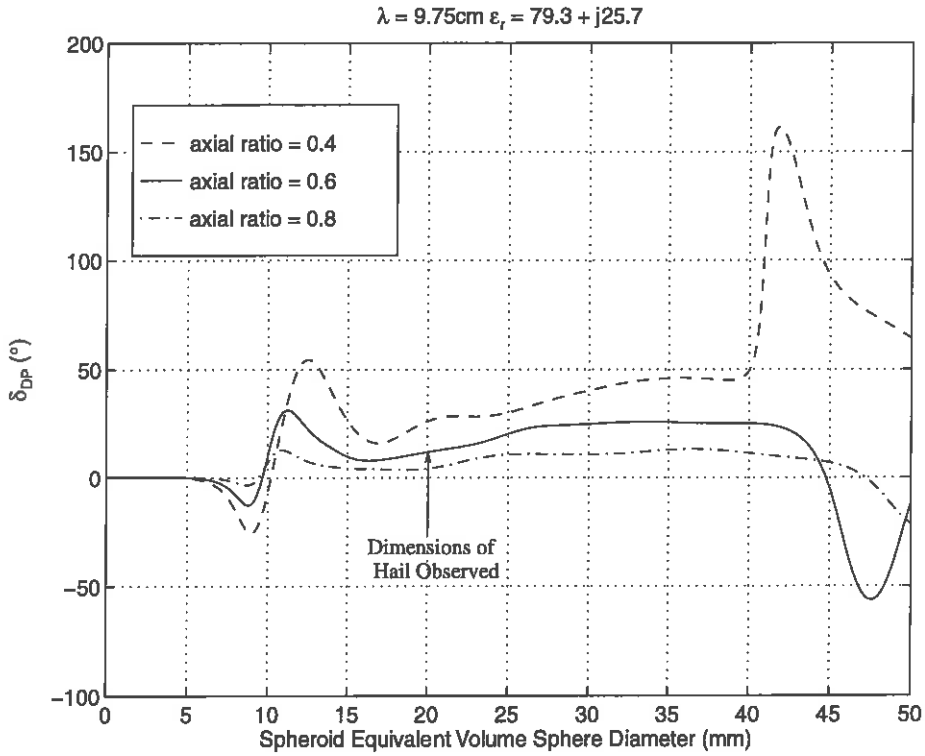

Figure 2:

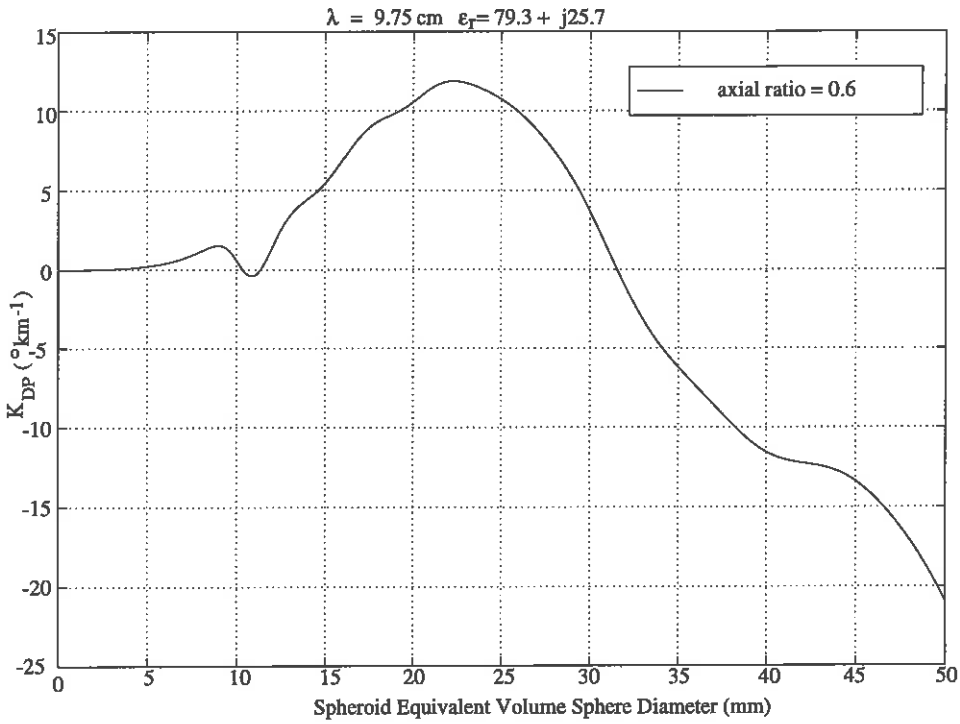

Figure 3:

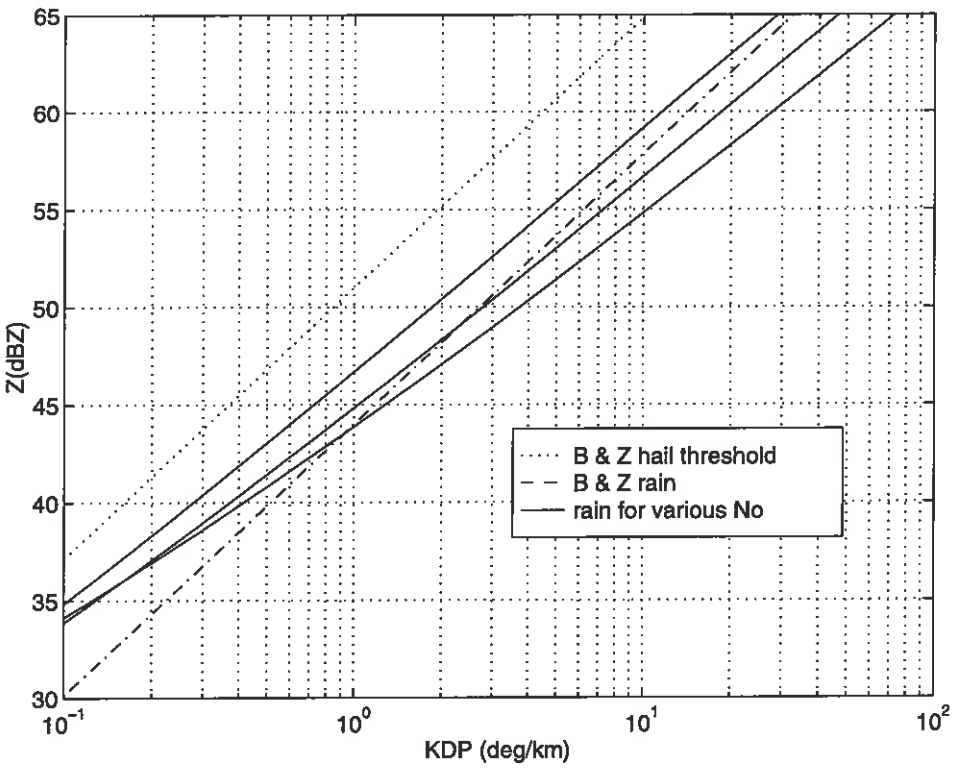
65
60
55
50
45
40
35
30
Z(dBZ)
10^{-1}
10^{0}
10^{1}
10^{2}
KDP (deg/km)
B & Z hail threshold
B & Z rain
rain for various No

Figure 4:

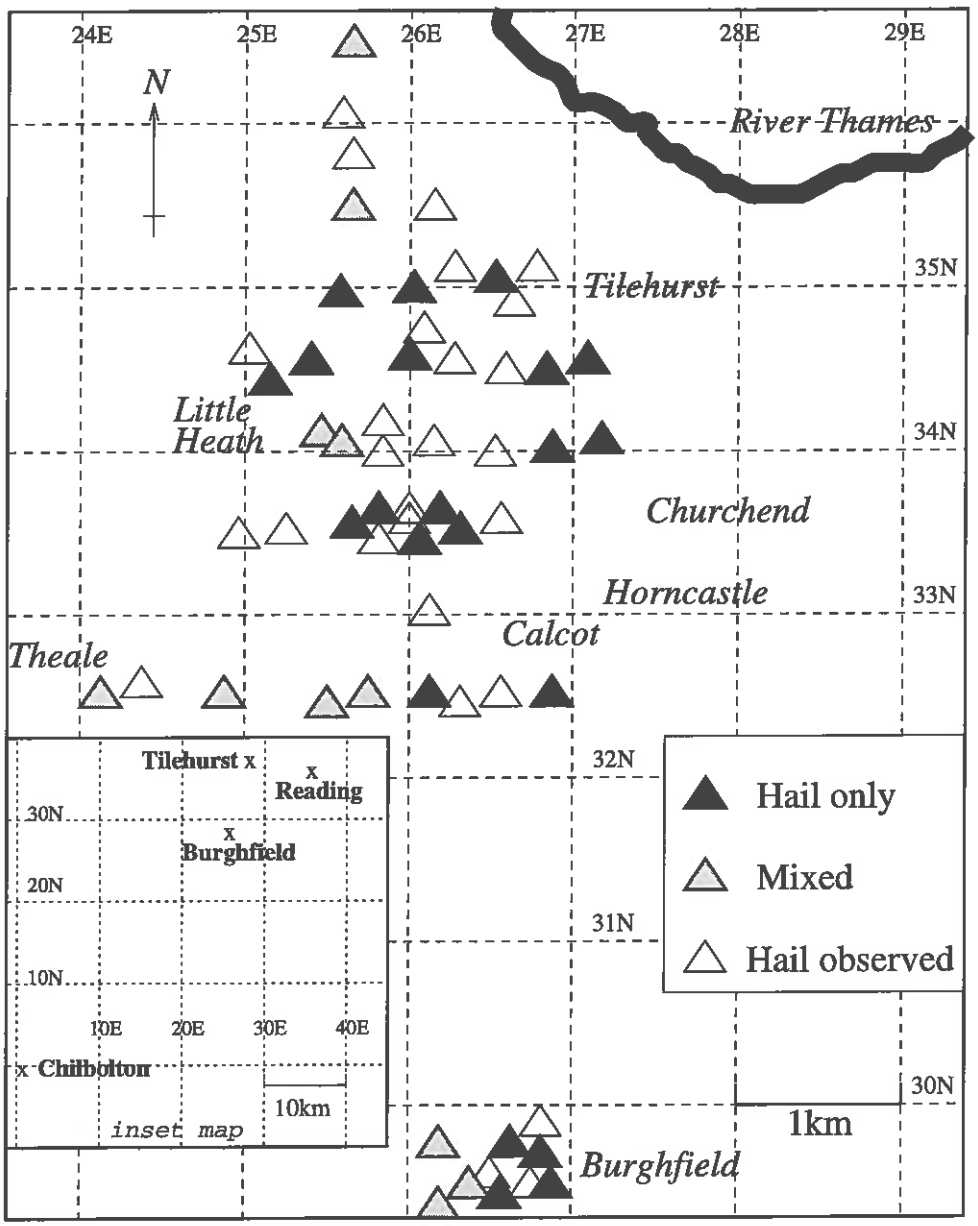
24E
25E
26E
27E
28E
29E
N
River Thames
35N
Tilehurst
Little
Heath
34N
Churchend
Horncastle
33N
Calcot
Theale
32N
Hail only
Mixed
Hail observed
31N
30N
1km
Burghfield
Tilehurst x
x
Reading
30N
x
Burghfield
20N
10N
10E
20E
30E
40E
x Chilbolton
10km
inset map

Figure 5:

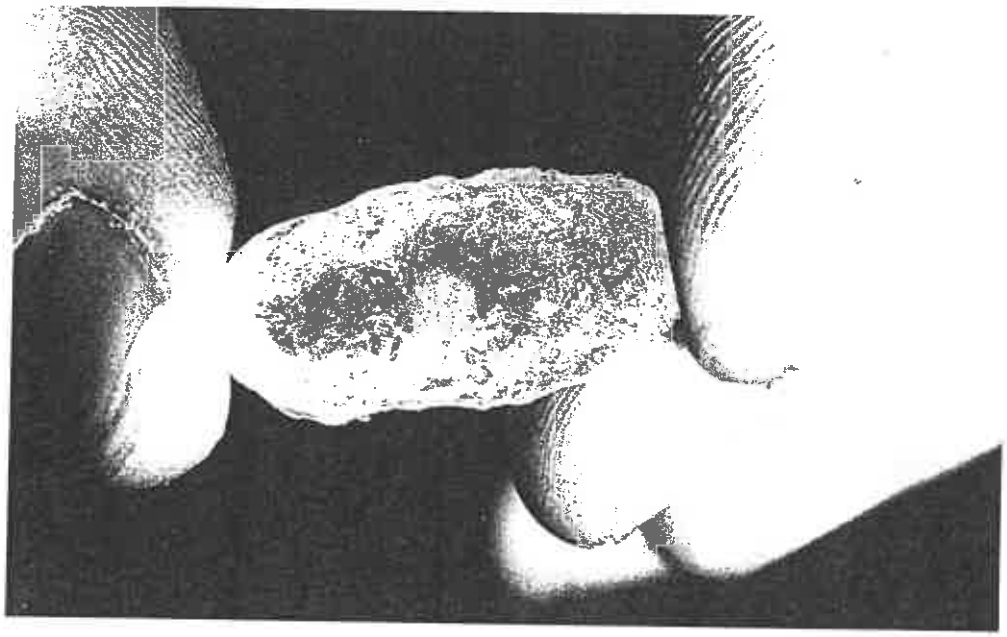

Figure 6:

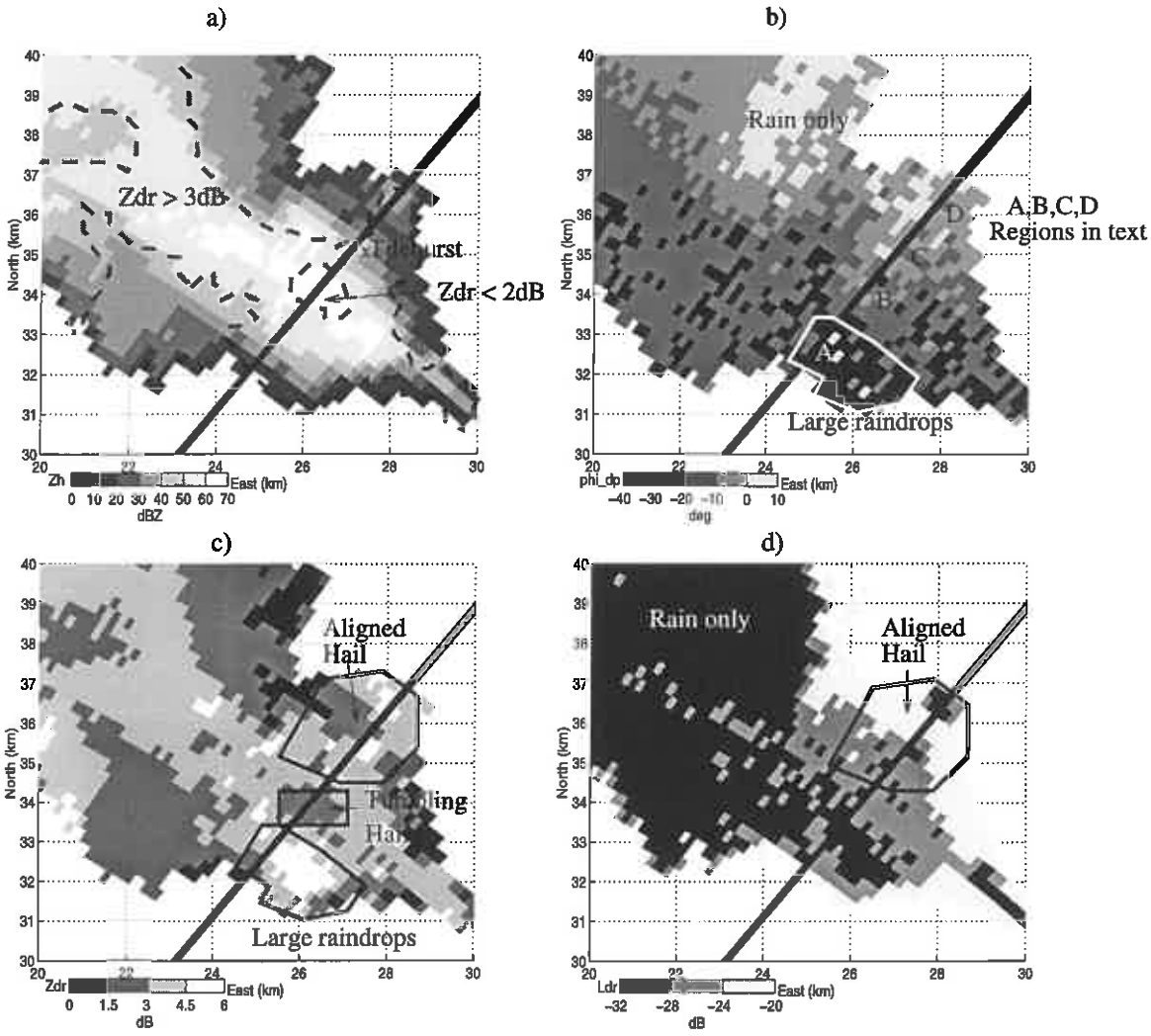
a)
b)
c)
d)
Zdr > 3dB
Zdr < 2dB
Rain only
A,B,C,D
Regions in text
Large raindrops
Aligned
Hail
Large raindrops
Rain only
Aligned
Hail
North (km)
East (km)
Zh
dBZ
phi_dp
deg
Zdr
dB
Ldr
dB

Figure 7:

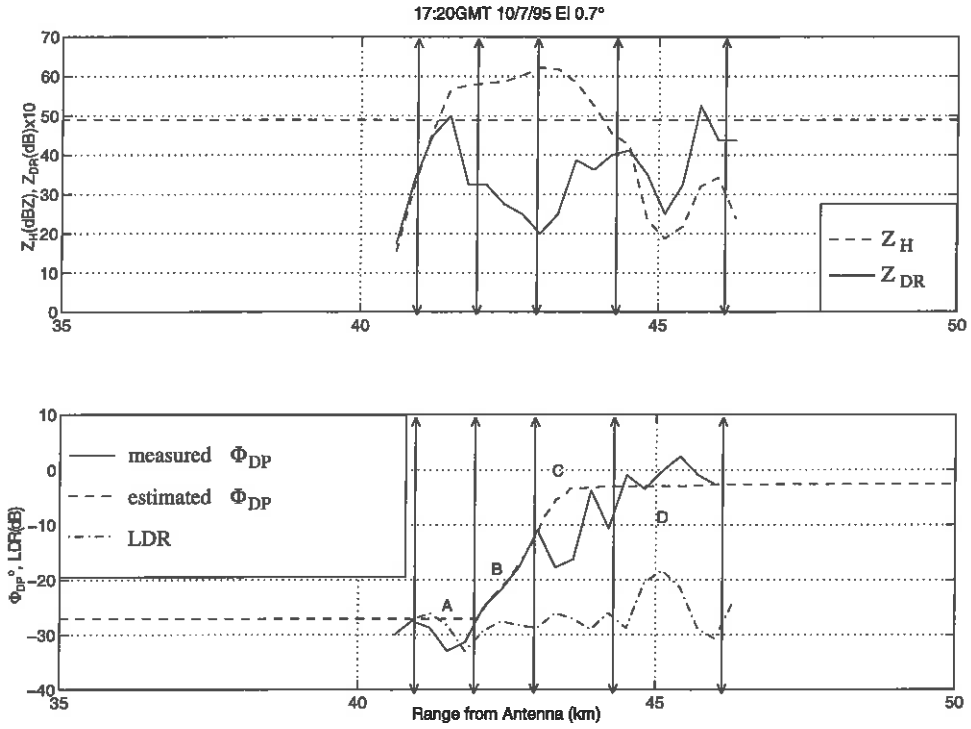

Figure 8:

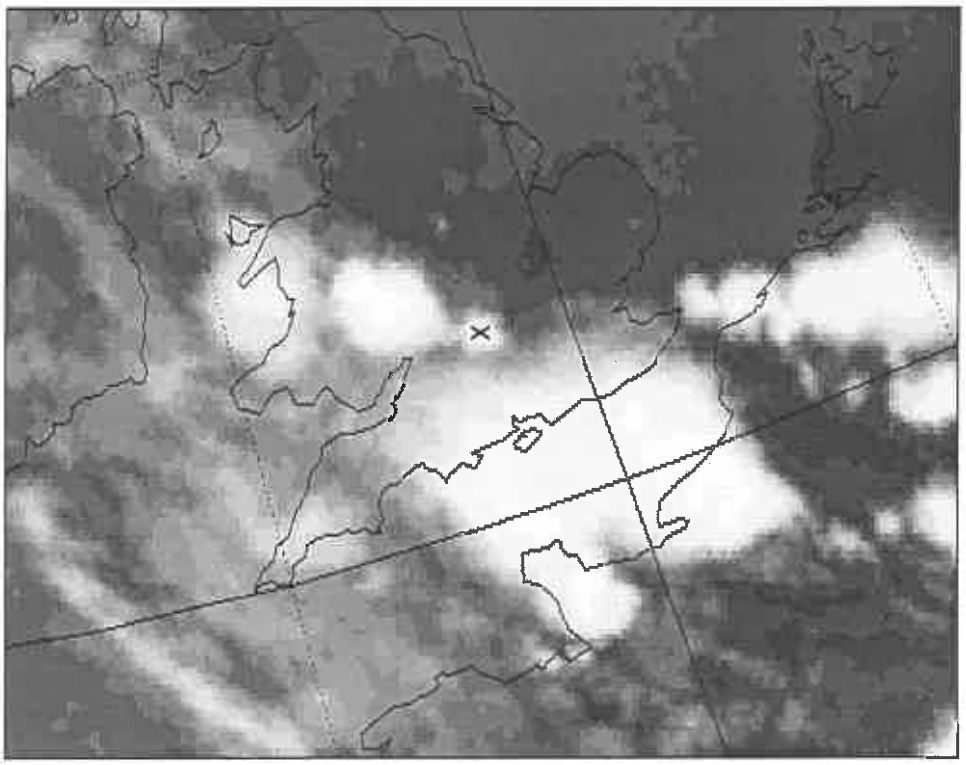

Figure 9:

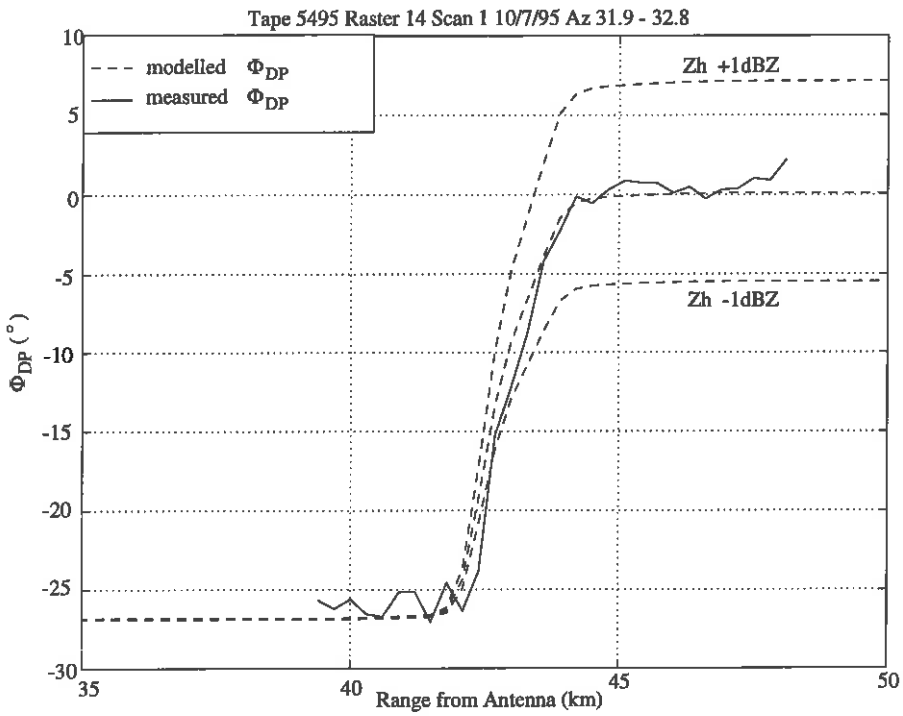
Tape 5495 Raster 14 Scan 1 10/7/95 Az 31.9 - 32.8
modelled Φ_{DP}
measured Φ_{DP}
Zh +1dBZ
Zh -1dBZ
Φ_{DP} (°)
10
5
0
-5
-10
-15
-20
-25
-30
35
40
45
50
Range from Antenna (km)

Figure 10:

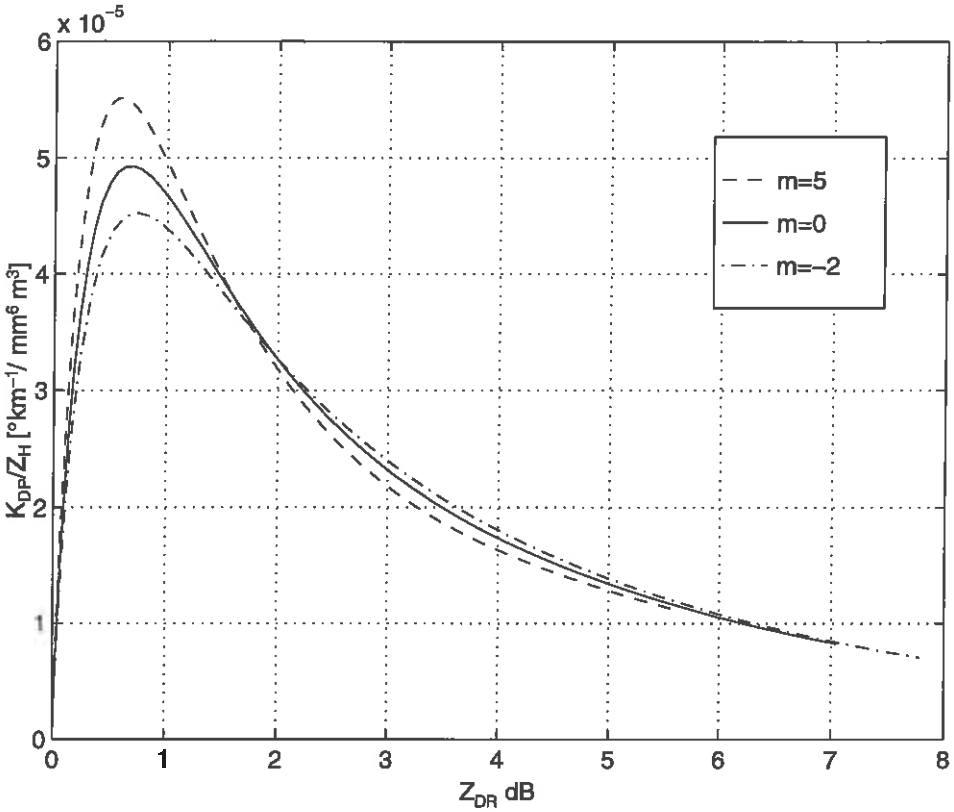

Figure 11:

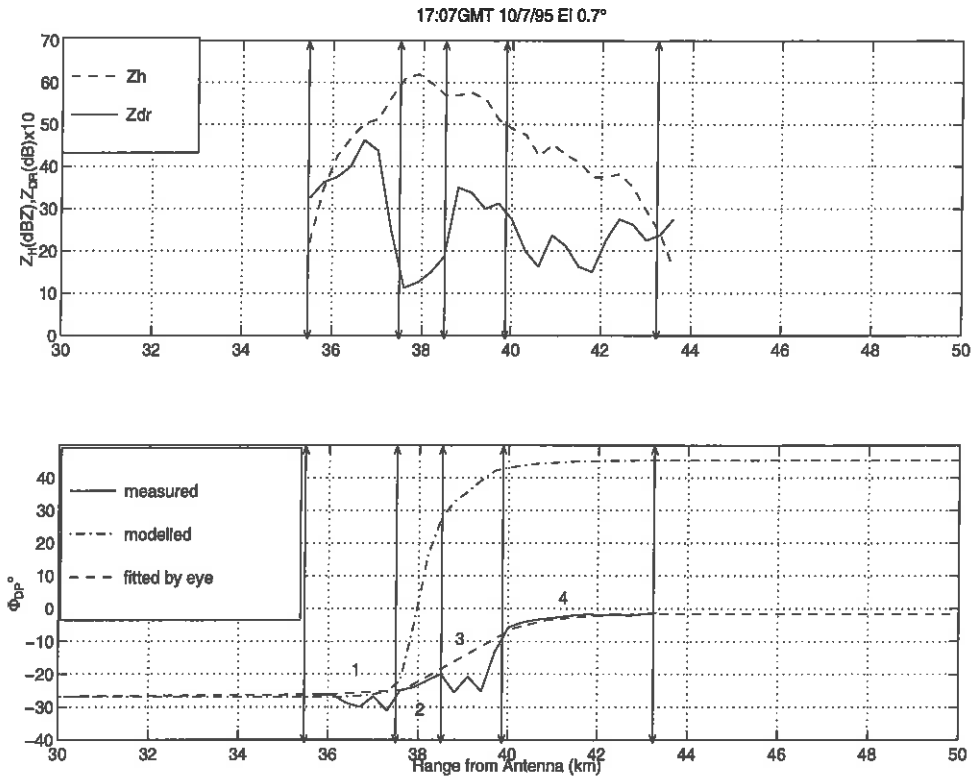

Figure 12:

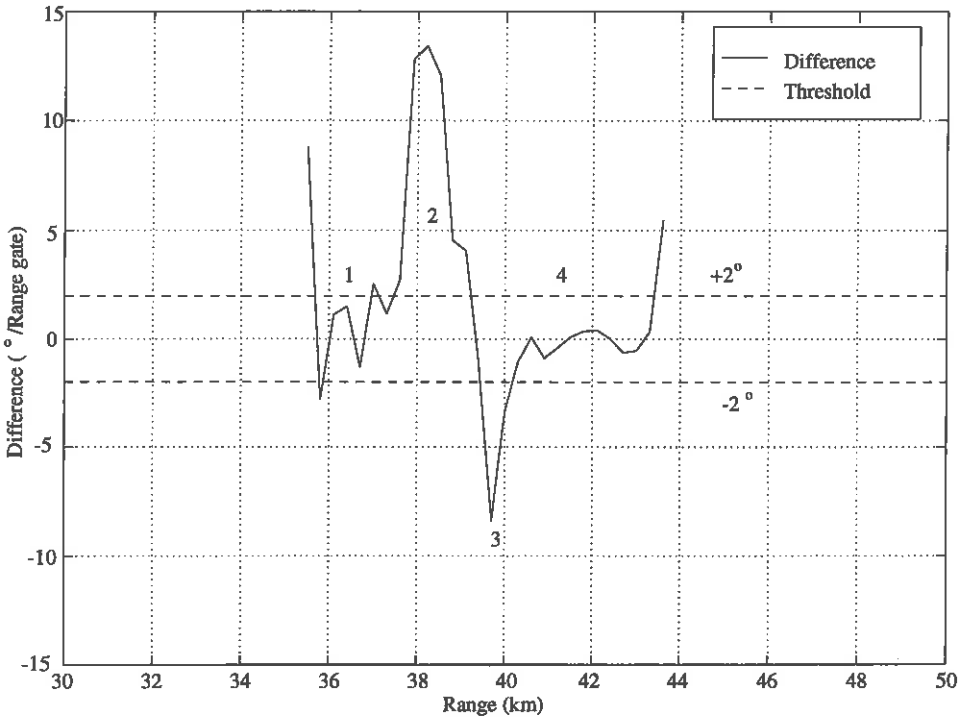

Figure 13:

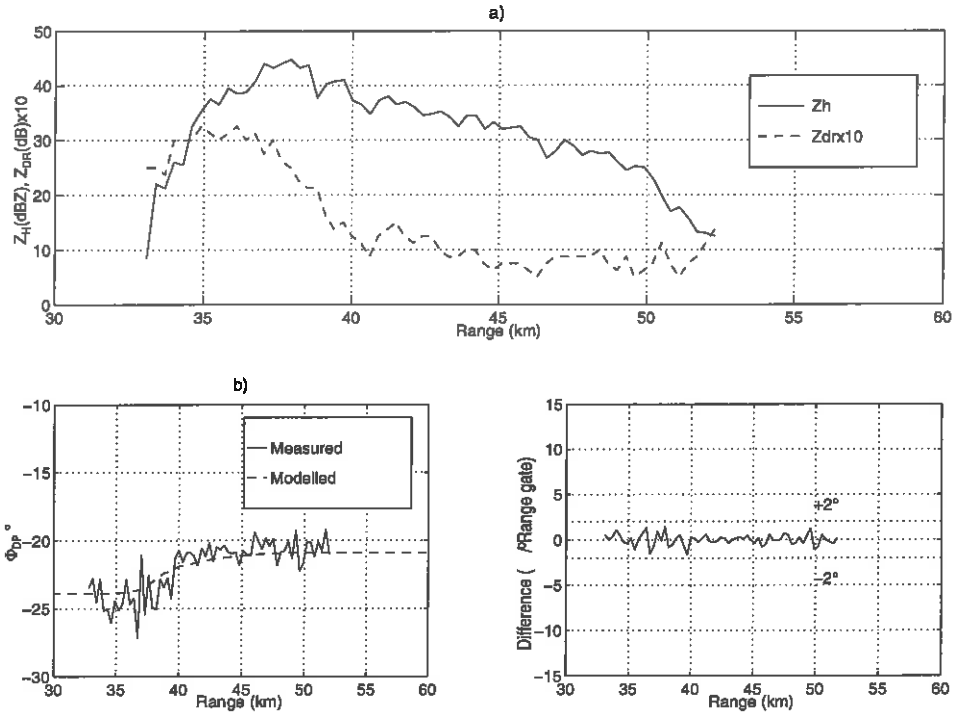

Figure 14:

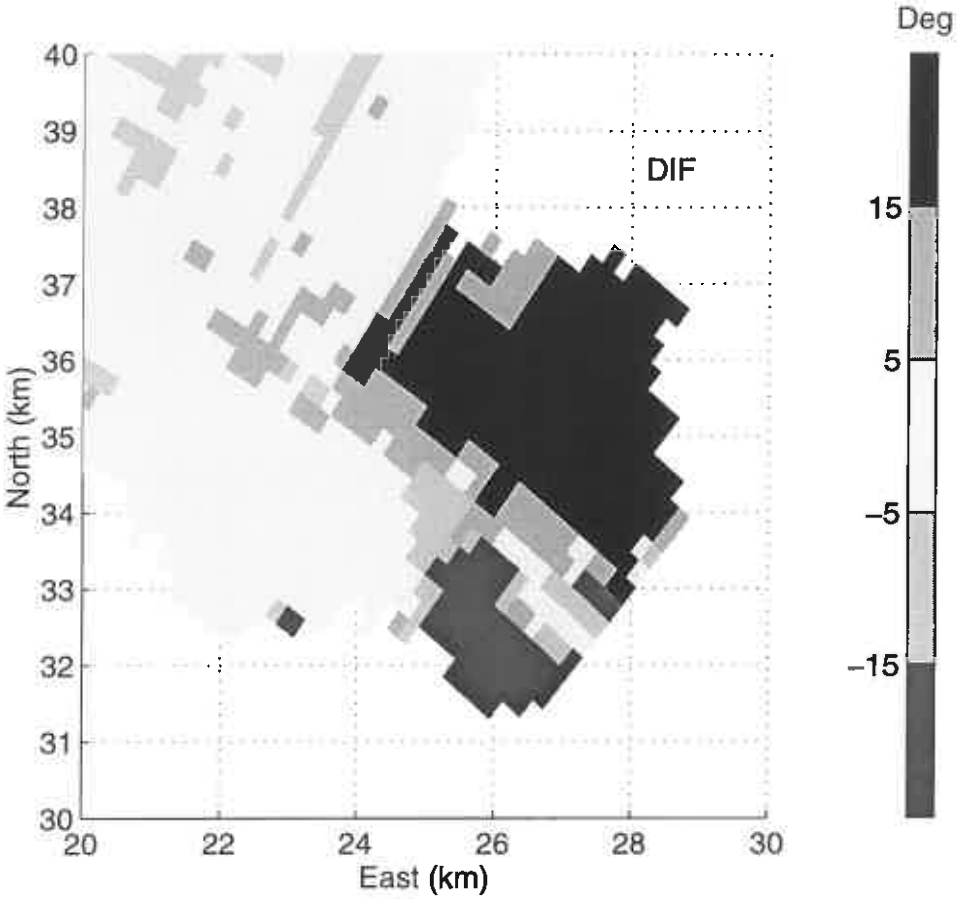

Figure 15:

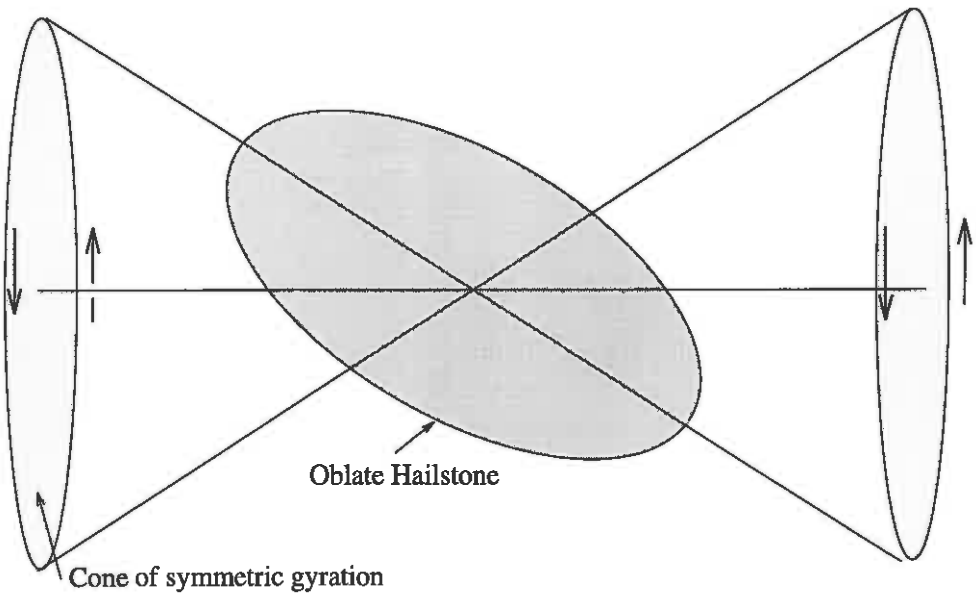

Figure 16:

CURRENT JCMM INTERNAL REPORTS

This series of JCMM Internal Reports, initiated in 1993, contains unpublished reports and also versions of articles submitted for publication. The complete set of Internal Reports is available from the National Meteorological Library on loan, if required.

1. **Research strategy and programme**
   K A Browning et al
   January 1993

2. **The GEWEX Cloud System Study (GCSS)**
   GEWEX Cloud System Science Team
   January 1993

3. **Evolution of a mesoscale upper tropospheric vorticity maximum and comma cloud from a cloud-free two dimensional potential vorticity anomaly**
   K A Browning
   January 1993

4. **The global energy and water cycle**
   K A Browning
   July 1993

5. **Structure of a midlatitude cyclone before occlusion**
   K A Browning and N Roberts
   July 1993

6. **Developments in systems and tools for weather forecasting**
   K A Browning and G Szejwach
   July 1993

7. **Diagnostic study of a narrow cold frontal rainband and severe winds associated with a stratospheric intrusion**
   K A Browning and R Reynolds
   August 1993

8. **Survey of perceived priority issues in the parametrizations of cloud-related processes in GCMs**
   K A Browning
   September 1993

9. **The effect of rain on longwave radiation**
   I Dharssi
   September 1993

10. **Cloud microphysical processes - a description of the parametrization used in the large eddy model**
    H Swann
    October 1993

11. **An appreciation of the meteorological research of Ernst Kleinschmidt**
    A J Thorpe
    May 1992

12. **Potential vorticity of flow along the Alps**
    A J Thorpe, H Volkert and Dietrich Heimann
    August 1992

13. **The representation of fronts**
    A J Thorpe
    January 1993

14. **A parametrization scheme for symmetric instability: test for an idealised flow**
C S Chan and A J Thorpe
February 1993

15. **The Fronts 92 Experiment: a Quicklook Atlas**
Edited by T D Hewson
November 1993

16. **Frontal wave stability during moist deformation frontogenesis**
Part 1: Linear wave dynamics
C H Bishop and A J Thorpe
May 1993

17. **Frontal wave stability during moist deformation frontogenesis**
Part 2. The suppression of non-linear wave development
C H Bishop and A J Thorpe
May 1993

18. **Gravity waves in sheared ducts**
S Monserrat and A J Thorpe
October 1993

19. **Potential vorticity and the electrostatics analogy: quasi-geostrophic theory**
C Bishop and A J Thorpe
November 1993

20. **Recent advances in the measurement of precipitation by radar**
A J Illingworth
April 1993

21. **Micro-physique et givrage: cloud microphysics and aircraft icing**
A J Illingworth
May 1993

22. **Differential phase measurements of precipitation**
M Blackman and A J Illingworth
May 1993

23. **Estimation of effective radius of cloud particles from the radar reflectivity**
N I Fox and A J Illingworth
May 1993

24. **A simple method of Dopplerising a pulsed magnetron radar**
A Hua, A J Illingworth and J Eastment
November 1993

25. **Radiation and polar lows**
George C Craig
February 1994

26. **Collected preprints submitted to the International Symposium on the Life Cycles of Extratropical Cyclones; Bergen, Norway, 27 June - 1 July 1994**
April 1994

27. **Convective frontogenesis**
Douglas J Parker and Alan J Thorpe
April 1994

28. **Improved measurement of the ice water content in cirrus using a total water evaporator**
Philip R A Brown and Peter N Francis
April 1994

29. **Mesoscale effects of a dry intrusion within a vigorous cyclone**
K A Browning and B W Golding
April 1994

30. **GEWEX Cloud System Study, Science Plan**
May 1994

31. **Parametrization of momentum transport by convectively generated gravity waves**
R Kershaw
May 1994

32. **Mesoscale Modelling Newsletter No 5**
May 1994

33. **Observations of the mesoscale sub-structure in the cold air of a developing frontal cyclone**
K A Browning, S A Clough, C S A Davitt, N M Roberts and T D Hewson
May 1994

34. **Longwave radiative forcing of a simulated tropical squall line**
Imtiaz Dharssi
July 1994

35. **On the nature of the convective circulation at a kata-cold front**
K A Browning
September 1994

36. **Collective preprints of papers submitted to the COST-75 International Seminar on Advanced Weather Radar Systems, Brussels, 20-23 September 1994**
November 1994

37. **Use of satellite imagery to diagnose events leading to frontal thunderstorms: Parts I and II of a case study**
K A Browning and N M Roberts
November 1994

38. **The role of spaceborne millimetre-wave radar in the global monitoring of ice cloud**
P R A Brown, A J Illingworth, A J Heymsfield, G M McFarquhar, K A Browning and M Gosset
December 1994

39. **Potential vorticity inversion**
Michal Ziemianski
October 1994

40. **Theory of mature tropical cyclones; a comparison between Kleinschmidt (1951) and Emanuel (1986)**
Suzanne L Gray
December 1994

41. **Dispersion and removal of pollutants during the passage of an atmospheric frontal system**
N R Gimson
December 1994

42. **The role of snow sublimation in frontogenesis**
D J Parker and A J Thorpe
December 1994

43. **Potential vorticity and the electrostatics Analogy: Ertel-Rossby formulation**
A J Thorpe and C H Bishop
December 1994

44. **Mesoscale aspect of extratropical cyclones: an observational perspective**
K A Browning
January 1995

45. **A polar low outbreak: evolution and mesoscale structures**
T D Hewson, G C Craig and C Claud
February 1995

46. **Generation of near-surface gusts of deep convection**
K Nakamura and R Kershaw
April 1995

47. **Attribution concepts applied to the Omega Equation**
S A Clough, C S A Davitt and A J Thorpe
June 1995

48. **Parametrization of mixed-phase cloud and precipitation**
Susan P Ballard and M Gerard Hutchinson
June 1995

49. **Short-range forecasting of stratocumulus: initialization prediction**
Susan P Ballard, Simon D Jackson and B Macpherson
June 1995

50. **Contributions of the JCMM/Dept of Meteorology Radar Group to the 27th AMS Radar Meteorology Conference, Vail October 1995**
June 1995

51. **Cold pools in shear**
Douglas J Parker
September 1995

52. **High-resolution analysis of frontal fracture**
K A Browning, S P Ballard and C S A Davitt
September 1995

53. **The albedo of broken cloud fields: calculations using a modified two stream radiation code**
Imtiaz Dharssi and Roy Kershaw
October 1995

54. **Parametrization of momentum transport by convection. I: theory and cloud modelling results**
R Kershaw and D Gregory
November 1995

55. **Variation of frontal structure along a cold front**
K A Browning and N M Roberts
November 1995

56. **Secondary frontal waves**
Douglas Parker
December 1995

57. **Objective fronts**
T D Hewson
March 1996

58. **Mesoscale analysis of the activation of a cold front during cyclogenesis**
K A Browning, N M Roberts and A J Illingworth
June 1996

59. **Investigation of different representations of rain in a 1-d evaporation model**
H Swann
May 1996

60. **Parametrization of diabatic processes in the inversion of the omega-equation**
M Athanassiadou and A J Thorpe
June 1996

61. **The role of the environmental flow in the development of secondary frontal cyclones**
I A Renfrew, A J Thorpe and A Joly
June 1996

62. **Consequences of the geostrophic momentum approximation on barotropic instability**
S Malardel, A J Thorpe and A Joly
June 1996

63. **Contributions to the AMS/RMS Conference on Mesoscale Processes**
Reading, 9-13 September 1996

64. **Vorticity and potential vorticity in stratified flows interacting with an isolated obstacle**
Jorge A Gutiérrez and A J Thorpe
September 1996

65. **Triple point development: two case studies**
Douglas Parker
September 1996

66. **Radar observations of wind-shear splitting within evolving atmospheric Kelvin-Helmholtz billows**
D Chapman and K A Browning
April 1997

67. **Cold frontal structure derived from radar wind profilers**
K A Browning, D Jerrett, J Nash, T Oakley and N M Roberts
May 1997

68. **The dry intrusion and its effect on the frontal, cloud and precipitation structure of extratropical cyclones**
K A Browning - Text of invited special lecture at the Spring Conference
of the Meteorological Society of Japan, University of Tsukuba, 22 May 1997

69. **Met. Office Unified Model data, diagnostics, graphics programs, and other observational data available from the JCMM through the aegis of the Universities Weather Research Network (UWERN).** (Plus supplement)
Peter Panagi and Ed Dicks
June 1997

70. **Contributions of the JCMM/Dept of Meteorology Radar Group to the 28th AMS Radar Meteorology Conference.** Austin, Texas
September 1997

71. **Sensitivity of short-range weather forecasts to local potential vorticity modifications**
Meral Demirtas and Alan Thorpe
July 1997

72. **Objective identification of frontal wave cyclones**
T D Hewson
August 1997

73. **Attribution and its application to mesoscale structure associated with tropopause folds**
A J Thorpe
September 1997

74. **The role of the environmental flow in the development of secondary frontal cyclones**
Ian A Renfrew, Alan J Thorpe and Craig H Bishop
September 1997

75. **Potential vorticity: a short history of its definitions and uses**
Alan J Thorpe and Hans Volkert
September 1997

76. **Superposing semi-geostrophic potential vorticity anomalies**
H R Birkett and A J Thorpe
September 1997

77. **Short period forecasting of catchment-scale precipitation.**
Part 1: the role of Numerical Weather Prediction
M A Pedder, M Haile and A J Thorpe
September 1997

78. **Verification of the tracking technique used in an experimental cloud motion wind inferring system**
Z Wang, K A Browning and G A Kelly
October 1997

79. **A preliminary study of Fourier series analysis for cloud tracking with GOES high temporal resolution images**
Z Wang
October 1997

80. **Analysis of an ex-tropical cyclone after reintensifying as a warm-core extratropical cyclone**
K A Browning, G Vaughan and P Panagi
November 1997

81. **A JCMM overview of FASTEX IOPs**
S A Clough, H W Lean, N M Roberts, H Birkett, J-P Chaboureau, R Dixon, M Griffiths, T D Hewson and A Montani
January 1998

82. **Programs for PV inversion and modification**
Meral Demirtas
December 1997

83. **Release of potential shearing instability in warm frontal zones**
D Chapman and K A Browning
February 1998

84. **The European Cloud-Resolving Modelling Programme (EUCREM)**
Summary Report from the coordinator
P W White
April 1998

85. **A frontal wave database**
T D Hewson
April 1998

86. **Layering observed in dropsoundings from IOP 1 of Fronts 92**
S A Clough
May 1998

87. **Use of wind-shear displays for Doppler radar data**
D Chapman and K A Browning
May 1998

88. **Radar estimates of rainfall rates at the ground in bright band and non-bright band events**
T J Smyth and A J Illingworth
June 1998

89. **Correction for attenuation of radar reflectivity using polarisation data**
T J Smyth and A J Illingworth
June 1998

90. **The effects of convection on chemical reactions and precipitation scavenging**
Neil R Gimson
July 1998

91. **How to use the display program DISP**
Nigel Roberts
August 1998

92. **Conceptual models of cyclogenesis**
Adrian T Semple
August 1998

93. **Observations of oblate hail using dual polarisation radar and implications for hail detection schemes**
T J Smyth, T M Blackman and A J Illingworth
September 1998

Met Office Joint Centre for Mesoscale Meteorology Department of Meteorology
University of Reading PO Box 243 Reading RG6 6BB United Kingdom
Tel: +44 (0)118 931 8425 Fax: +44 (0)118 931 8791
www.metoffice.com